Journal of
Materials Chemistry B

ROYAL SOCIETY OF CHEMISTRY

Novel iron oxide-cerium oxide core-shell nanoparticle as a potential theranostic material for ROS-related inflammatory diseases

Novel iron oxide-cerium oxide core-shell nanoparticle as a potential theranostic material for ROS related inflammatory diseases

Yuao Wu[a], Yanchen Yang[a], Wei Zhao[a], Zhi Ping Xu[a], Peter Little[d], Andrew K. Whittaker[a,b,c], Run Zhang[a], Hang T. Ta[a,b,d*]

[a]Australian Institute for Bioengineering and Nanotechnology, The University of Queensland, Brisbane, Australia

[b]Australian Research Council Centre of Excellence in Convergent Bio-Nano Science and Technology, Brisbane, Australia

[c]Centre for Advanced Imaging, the University of Queensland, Brisbane, Australia

[d]School of Pharmacy, the University of Queensland, Brisbane, Australia

*Correspondence to Hang T. Ta (h.ta@uq.edu.au)

Novel iron oxide-cerium oxide core-shell nanoparticle as a potential theranostic material for ROS related inflammatory diseases

Abstract

Reactive oxygen species (ROS) and reactive nitrogen species (RNS) are key signaling molecules that play an important role in inflammation and progression of many diseases such as cardiovascular disease, especially atherosclerosis. ROS are in particular a significant factor in the development of rheumatoid arthritis and other autoimmune diseases such as allergies. In this study, novel Fe_3O_4/CeO_2 core-shell theranostic nanoparticles capable of reacting with ROS and of being detected by MRI were synthesized and thoroughly characterized. *In vitro* studies, such as measurement of cell uptake, magnetic resonance imaging, toxicity and ROS scavenging were conducted. The results indicate that the novel Fe_3O_4/CeO_2 theranostic nanoparticles are effective at scavenging ROS and show excellent magnetic resonance (MR) imaging performance. These theranostic nanomaterials, therefore, show great potential for the treatment and diagnosis of ROS-related inflammatory diseases.

Keywords: ROS-related inflammatory disease, theranostics, iron oxide, cerium oxide, magnetic resonance imaging.

Introduction

Inflammatory diseases comprise a group of diseases that involve the body's immune system. Diseases such as rheumatoid and atherosclerosis affect many millions of people every year. For example, atherosclerosis, the most prevalent cardiovascular diseases, may cause ischemic heart disease and cerebrovascular disease (stroke).[1] In 2013, ischemic heart disease and cerebrovascular disease are claimed to be the world's first and third cause of death, causing 137 and 110 deaths per every 100,000 people respectively.[2] Also, more than half of patients with rheumatoid arthritis are incapable of holding a full-time job as a direct consequence of the disease.[3]

Reactive oxygen species (ROS) production is one of the main reason for the progression of many inflammatory diseases. ROS includes hydrogen peroxide (H_2O_2), superoxide, and hydroxyl radicals as well as their reactive products; those molecules contain a high level of reactive oxygen described as harmful products of metabolism.[4] H_2O_2 is the most important ROS in redox signaling among those. In addition, it is the most studied and the best-characterized member of ROS.[5] Due to their oxidization capability, ROS are able to damage important molecules in our bodies, such as lipid peroxidation, DNA mutation, and protein dysfunction.[5, 6] Therefore, ROS are key signaling molecules that play an important role in the progression of inflammatory disorders. In addition to their potential harm, it is reported that ROS are regulators of cell signaling and immune responses.[7]

There are four kinds of ROS in the inflammation diseases, the most important of which is NADPH oxidase-derived ROS that relates to both atherosclerosis[5, 8] and rheumatoid arthritis[6]. Besides, there are also mitochondrial-derived ROS[5, 9], uncoupled nitric oxide synthase-derived ROS[10] and xanthine oxidoreductase derived ROS[11] in inflammatory diseases. Under the inflammatory conditions, the oxidative stress produced by polymorphonuclear neutrophils such

as macrophages leads to the formation of inter-endothelial junctions, accelerating the migration of inflammatory cells across the endothelial barrier, which makes the situation worse in atherosclerosis and rheumatoid arthritis patients.[12, 13] In atherosclerosis, ROS is produced by macrophages and endothelial cells during the process of the plaque, and it is the key factor of the accumulation of oxidized low-density lipoprotein in the intima of the blood vessel.[14, 15] In rheumatoid arthritis, the relevant ROS including nitric oxide (NO) and superoxide anion (O^{2-}) is produced by chondrocytes followed by the generation of derivative radicals, such as hydrogen peroxide (H_2O_2).[16, 17] Therefore, an effective antioxidant compound, which can reduce ROS in the inflammatory cells, could be a key factor for the treatment of chronic inflammatory disease.

Cerium compounds have been used as traditional drugs for inflammation over the last two hundred years. The first publication of cerium used as drugs can trace back to 1850s. Originally, the trivalent ions of cerium were used to treat bacterial infections, sepsis and inflammatory responses in patients with fire burns.[18] In 2007, Korsvik et al. demonstrated that higher levels of Ce^{3+} than Ce^{4+} on the surface of the particle are more likely to act as superoxide dismutase, which accelerates the dismutation of superoxide radical to O_2 or H_2O_2.[19] This ability of anti-superoxide radical is supported by another study claiming that high Ce^{3+}/Ce^{4+} ratio of nanoparticles contributes more superoxide dismutase activities than low Ce^{3+}/Ce^{4+} ratio. [20] The potential mechanism of the unique regeneration antioxidant property of cerium oxide is illustrated in figure 1A, which results from the switch between Ce^{3+} and Ce^{4+} on the surface of the nanoparticle.[21, 22] Therefore, cerium oxide nanoparticles with their unparalleled antioxidant properties are potential radical scavengers and redox cycling antioxidants.

Superparamagnetic iron oxide nanoparticles (SPIONs) are small synthetic particles with Fe_2O_3 or Fe_3O_4 cores. SPIONs usually range between 10 nm and 100 nm in diameter and are excellent contrast agents for the magnetic resonance imaging.[23] SPIONs are usually coated with

biocompatible polymers, such as polyethylene glycol, limiting their interaction with substances in the surrounding environment and enhancing their stability in physiological conditions.[24] In ROS related inflammatory diseases, molecule markers such as chemokines, cytokines and other adhesion molecules, take part in the inflammation process.[25] Recently, in atherosclerosis,[26] iron oxide nanoparticles functionalized with binding ligands that target atherosclerosis biomarkers have been widely studied as molecular magnetic resonance imaging (MRI) of atherosclerosis.[17, 18] SPIONs can be a potential imaging agent for diagnosing inflammatory diseases as well as monitoring treatment of these diseases.

Nanotechnology has taken the most important place in the development of theranostics which exhibits not only effective therapy but also imaging for many diseases such as cancer and inflammatory disease.[27, 28] Basically, theranostic nanoparticles are capable of loading large amounts of therapeutic and imaging agents as well as banding functional targeting ligands at the surface, which can increase the therapeutic and imaging efficacy while reducing off-site toxicity.[29] Functionalization of theranostic nanoparticles can modulate the drug release related to the internal environment in our bodies such as temperature, enzymes, the potential of hydrogen (pH) value and redox potential.[30] The half-life time of the theranostic nanoparticles can be enhanced by modification of the surface by hydrophilic polymer such as poly (acrylic acid) (PAA).[29] Theranostic nanomaterials combine both diagnostic and therapeutic capabilities in one dose, and also allow the tracking or monitoring of drug delivery to the disease site.

In this study, we have synthesized a novel theranostic nanoparticle comprising an iron oxide (core) and cerium oxide (shell) (Figure 1B) as a potential theranostic nanomaterial for ROS related inflammatory diseases. This innovative nanomaterial simultaneously provides both diagnostic capability via iron oxide (MR imaging agent) and therapeutic functionality via cerium oxide (anti-ROS capability) in one dose. This combination is also expected to allow the

tracking of cerium oxide delivery to the disease site and enable its biodistribution evaluation. The characterization studies indicated that these iron oxide-cerium oxide core-shell nanoparticles (IO@CO) are good contrast agents for MRI. *In vitro* studies showed that our nanoparticles have the significant anti-ROS ability with good cell uptake and low cytotoxicity. These IO@CO nanoparticles could be a potential agent for diagnosis and treatment of ROS-related inflammatory diseases such as atherosclerotic plaques and rheumatoid arthritis.
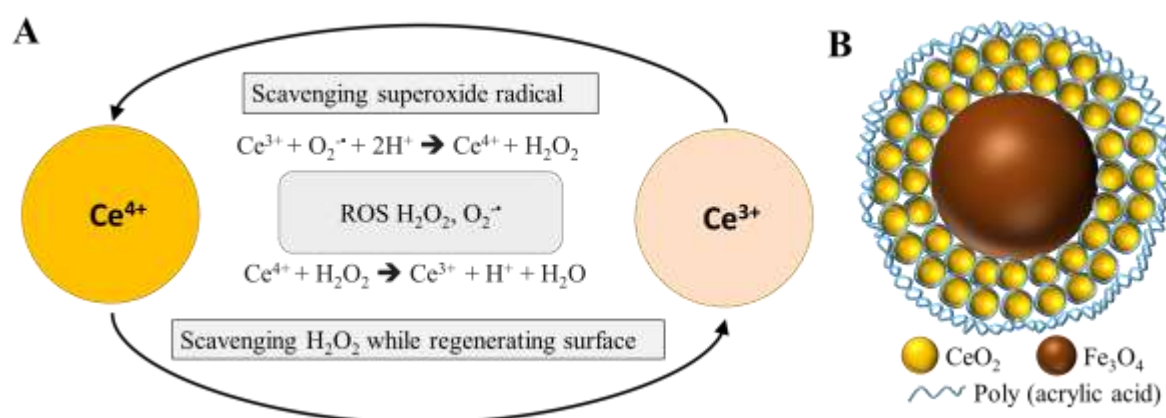

Figure 1. Regenerative antioxidant property of cerium oxide and simulation structure of iron oxide/cerium oxide core-shell nanoparticles (IO@CO) (A) Regenerative antioxidant property of cerium oxide shows that cerium ions are capable of scavenging superoxide radical when the trivalent cerium ions change to tetravalent cerium ions[21]. On the other hand, it has the ability of scavenging H_2O_2 when tetravalent cerium ions become trivalent cerium ions. (B) Simulation structure of iron oxide/cerium oxide core-shell nanoparticles (IO@CO).

Experimental section

Materials

Iron chloride, sodium oleate, polyoxyethylene (5) nonylphenyl ether (Igepal CO-520), cerium nitrate hexahydrate, urea, poly (acrylic acid) (PAA, Mw=1800), Hydrogen peroxide (H_2O_2), 2,2'-azino-bis(3-ethylbenzothiazoline-6-sulphonic acid) (ABTS), horseradish peroxidase (HRP) and 2',7'-Dichlorodihydrofluorescein diacetate (DCFH-DA) were purchased from Sigma-Aldrich. Water used in all experiments was Milli-Q water. Phosphate-buffered saline (PBS), RPMI 1640 Medium, fetal calf serum, penicillin-streptomycin solution, L-glutamine, non-

essential amino acids solution (100X) and TrypLE™ Express were purchased from ThermoFisher Scientific. Ethodium homodimer-1 fluorescence dye was purchased from Molecular Probes™.

Synthesis of iron-oleate complex

Iron-oleate complexes were synthesized according to previous report[31]. Typically, 44.6 g of sodium oleate (120 mmol, ≥82%) and 10.8 g of iron chloride ($FeCl_3 \cdot 6H_2O$, 40 mmol, 98%) was dissolved in a mixture solvent composed of 80 ml ethanol, 60 ml distilled water and 140 ml hexane. The resulting solution was heated to 70°C and kept at this temperature for four hours. When the reaction was completed, the upper organic layer containing the iron-oleate complex was washed three times with 30 ml distilled water in a separatory funnel. After washing, hexane was evaporated off, resulting in iron-oleate complex in a viscos liquid form.
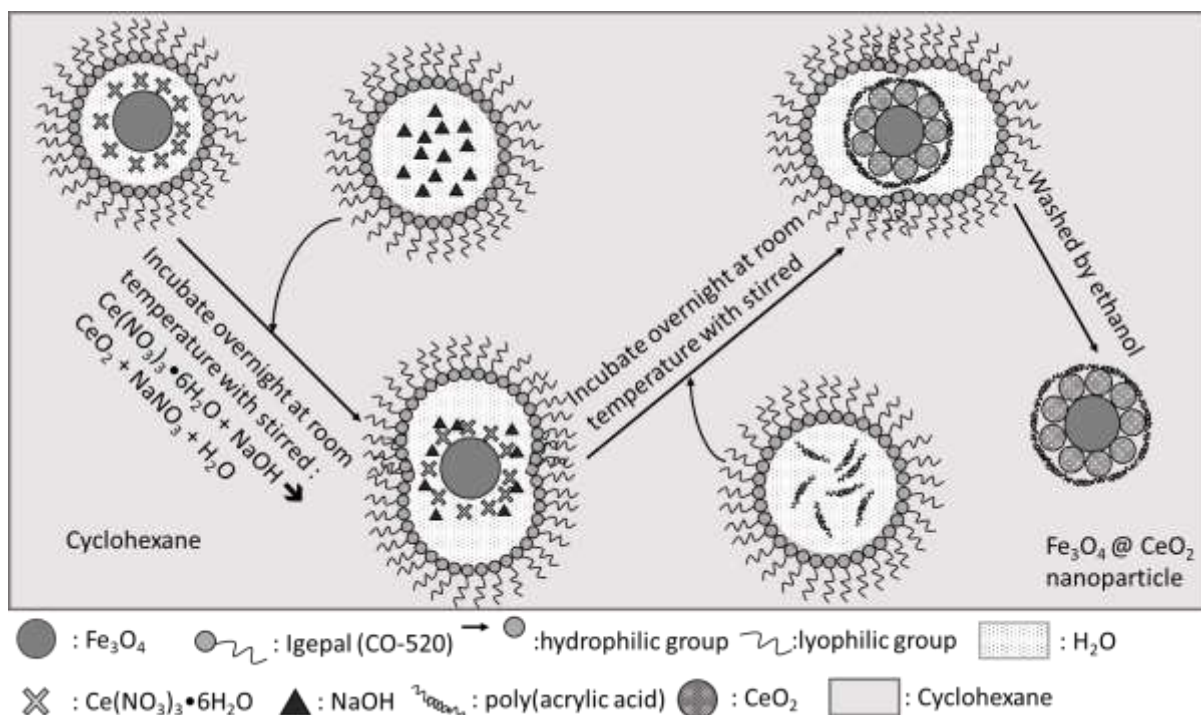
Synthesis of iron oxide nanoparticle

Fe_3O_4 nanoparticles with core size of 10 nm were synthesized according to a previous report with slight modifications[32]. Typically, 3.6 g (4 mmol) of freshly prepared iron oleate and 3.39 g (4 mmol) of oleic acid were dissolved in 25 ml of 1-octadecence. The resultant solution was degassed for 10 min using argon and then was heated to 310°C for 1 hour under argon protection. The preparation was terminated by cooling the reaction mixture to room temperature (RT). The nanoparticles were washed three times by precipitation with ethanol and redispersion in cyclohexane.

Synthesis of iron oxide/cerium oxide core-shell nanoparticles (IO@CO)

Synthesis of IO@CO1 (NaOH used as precipitation agent). Reverse micelle systems were used to synthesize IO@CO nanoparticles. Firstly, the $Fe_3O_4/Ce(NO_3)_3$ reverse micelle solution was prepared as follows. 0.96 g Igepal CO-520 (2.185 mmol) (sonication for 30min after adding into cyclohexane) and 0.6 mg Fe3O4 nanoparticles were dispersed in 10.5 ml of
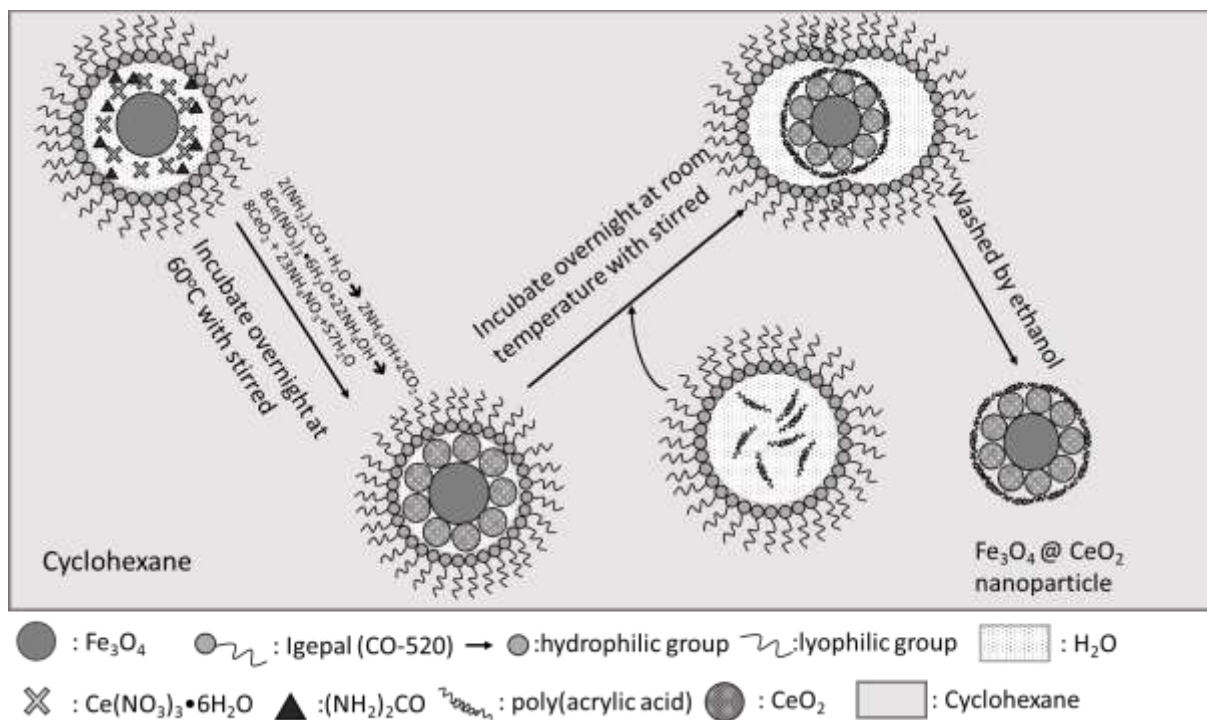
cyclohexane and gently stirred for 2 h at RT. After 2 h, 0.04g $Ce(NO_3)_3 \cdot 6H2O$ (0.92 M) was dispersed in 100 μl water, and the solution was labeled as mixture A. Then 100 μl of mixture A was added to above solution and the mixture was vigorously stirred for 2 hours. Secondly, the NaOH reverse micelle solution was prepared as follows. 0.48 g Igepal CO-520 (1.0925 mmol) (sonication for 30min after adding into cyclohexane) was dispersed in 5.25 ml of cyclohexane. Then, solution B containing 50 μl NaOH aq. (1.5 M) was added to above mixture and the solution was vigorously stirred for 2h at RT. The two reverse micelle solutions were blended and incubated overnight at RT with stirring at 250 rpm. After 24 h, the poly(acrylic acid) reverse micelle solution was prepared as follows. 0.48 g Igepal CO-520 (1.0925 mmol) (sonication for 30min after adding into cyclohexane) was dispersed in 5.25 ml of cyclohexane. Next, 2 mg poly(acrylic acid) dissolving in 50 μl water was added to the reaction solution, and the solution was stirred vigorously for 2h at RT. After 2h, the poly(acrylic acid) reverse micelle solution was added to the mixture of two reverse micelle solutions that had been incubated overnight. The mixture containing three reverse micelle solutions was stirred overnight at 250 rpm. After that, the nanoparticles were precipitated by adding 2 ml methanol and separated by high speed centrifugation (20,000 rpm, 15 min, 22°C). The precipitate was washed twice with 1 ml ethanol and subsequently washed once with a mixture of water and ethanol (500 μl: 500 μl). The resultant nanoparticles (IO/CONP1) were washed by dialysis, and then concentrated and redispersed in 100 μl water. Scheme 1 illustrates the synthesis protocol of IO@CO1)

Scheme 1: Image illustrating the synthesis of IO@CO1. The protocol including (1) Igepal CO-520 and Fe$_3$O$_4$ nanoparticles were dispersed in cyclohexane and stirred for 2h at RT. Ce(NO$_3$)$_3$•6H$_2$O was added into the above solution and stirred for another 2h at RT. (2) Igepal CO-520 and NaOH were dispersed in cyclohexane and stirred for 2h at RT. The first and second solutions were mixed and incubated overnight at RT with stirring. (3) Igepal CO-520 and poly(acrylic acid) were stirred for 2h at RT and added into mixed solution above. The mixture was then incubated overnight at RT with stirring. After incubation, nanoparticles were washed and redispersed in water.

Synthesis of IO@CO2 (urea used as precipitation agent). Firstly, the Fe3O4/ Ce(NO$_3$)$_3$/ (NH$_2$)2CO reverse micelle solution was prepared as follows. 0.96 g Igepal CO-520 (2.185 mmol) (sonication for 30min after adding into cyclohexane) and 0.6 mg Fe3O4 nanoparticles were dispersed in 10.5 ml of cyclohexane and gently stirred for 2h at RT. After 2h, 0.005g Ce(NO$_3$)$_3$•6H2O (0.58 M), 0.0075g (NH$_2$)2CO (6.2 M) were dispersed in 20 μl water, and the solution was labeled as mixture A. Then 20 μl of mixture A was added above solution, and the solution was vigorously stirred for 2 h. After 2h, the mixture was heated at 60°C overnight with gentle stirring. After 24 h, the poly(acrylic acid) reverse micelle solution was prepared as follows. 0.48 g Igepal CO-520 (1.0925 mmol) (sonication for 30min after adding into

cyclohexane) was dispersed in 5.25 ml of cyclohexane. Next, 2 mg poly(acrylic acid) dissolving in 50 μl water was added to the reaction solution, and the solution was stirred for 2h at RT. The two reverse micelle solutions were mixed together and vigorously stirred for 2h. Then, the stirring speed was reduced to 250 rpm and the reaction solution was incubated overnight at RT with gentle stirring. After that, the following steps were the same as that of IO/CO1, including precipitation, washing, dialysising and concentrating. Finally, the nanoparticles (IO@CO2) were redispersed in 100 μl water. Scheme 2 illustrates the synthesis of IO@CO2.

Scheme 2: Image illustrating the synthesis of IO@CO2. The protocol including (1) Igepal CO-520 and Fe_3O_4 nanoparticles were dispersed in cyclohexane and stirred for 2h at RT. $Ce(NO_3)_3 \cdot 6H_2O$ and $(NH_2)_2CO$ were added and stirred for another 2h at RT. (2) The solution was incubated for 24h at 60°C with stirring. After that, Igepal CO-520 and poly(acrylic acid) were stirred for 2h at RT and then added into solution above and stirred for another 2h. The synthesised nanoparticles were washed and redispersed in water.

Characterisation of nanoparticles:

Transmission electron microscopy (TEM) images were collected on a JEOL-JEM-1010 Transmission Electron Microscope operating at an accelerating voltage of 100 kV. Hydrodynamic size, size distribution and zeta potential (ZP) of the nanoparticles were measured using a Zetasizer Nano ZS (Malvern). The iron and cerium concentrations of IO@CO were determined by inductively coupled plasma-optical emission spectroscopy (ICP-OES) (Optima 8300DV ICP-OES from Perkin Elmer). Fourier Transform Infrared Spectroscopy (FTIR) spectra were collected using a Nicolet 5700 FT-IR. The surface composition of the nanoparticle was analyzed by X-ray Photoelectron Spectroscopy (XPS) using a Kratos Axis Ultra photoelectron spectrometer. T_1 relaxation time of nanoparticles was recorded on a Avance 400 MHz spectrometer. T_2 relaxation time and magnetic resonance imaging (MRI) of nanoparticles were measured with a Bruker 9.4T MRI scanner. T_2-weighted relaxivity (r_2) are generally defined as the slope of the linear regression generated from a plot of the measured relaxation rate ($1/T_2$) versus the concentration of the contrast agent (iron, Fe).

Anti-ROS capability of IO@CO nanoparticles

Nanoparticles of different cerium (Ce) concentrations (0μg/ml, 0.0028μg/ml, 0.028μg/ml 0.28μg/ml, 2.8μg/ml, 5.6μg/ml, 11.2μg/ml) were treated with 0.1mM H_2O_2 in 96-well plate for 1h at 37°C with shaking (200 rpm). 0.01 unit of HRP was added into each reaction followed by 10 min incubation at RT. 8.7mM of ABTS was then added into the reaction and the absorbance of samples at 405 nm was measured by microplate reader Tecan X200. The absorbance of 0μg/ml sample was determined as 0% ROS scavenging.

Cell culture

Macrophage J774A.1 was attained from the American Type Culture Collection (ATCC). The cells were maintained in non-treated 100×20mm cell culture dish containing RPMI 1640 with

fetal calf serum (10%), penicillin (100 U/mL) and L-glutamine (1%) and cultured in an incubator at 37 °C with 5% CO_2.

Cell uptake of IO@CO nanoparticles

When cell confluence reached approximately 90%, the cells were detached using cold PBS (4°C) by pipette. Then cells were transferred to 24-well plate at a density of 40000 cells/well. After 48 h incubation, cells were separately treated with different concentrations of IO@CO1 and IO@CO2 ([Ce]: 0μg/ml, 2.8μg/ml and 5.6μg/ml). After an additional 24 h incubation, cells in the 24-well plate were washed by 1xPBS and then lysed by 8% HNO_3 and the lysis solutions were diluted to 2% HNO_3 for Inductively coupled plasma mass spectrometry (ICP-MS) (Agilent 7900 with collision cell technology) analysis. ICP-MS was used to detect the content of Fe and Ce in macrophages treated with different concentrations of the nanoparticles.

In vitro MRI

When cell confluence reached approximately 90%, the cells were detached using cold PBS (4°C) by pipette. Cells were then transferred into 96-well plate at a density of 5000 cells/well. After 48 h incubation, cells were separately treated with different concentration of IO@CO1 and IO@CO2 ([Ce]: 2.8μg/ml). After an additional 24 h incubation, cells were washed with PBS twice and the fixed by paraformaldehyde (PFA). The cells were detached by TrypLE Express and centrifuged for MRI. To prepare the MRI samples, cells were centrifuged at 200g for 5min in a 1.5ml eppendorf tube and resuspended in 10μl of 0.5% agarose solution to make the cell-containing gel. After the solidification of the cell pellet, 0.5% agarose gel was added at the top of the cells pellet and the 1.5ml eppendorf tube was placed in the 50ml centrifuge tube containing 0.5% agarose gel (Scheme 3). MRI samples were prepared as shown in scheme 3 followed by imaging using 9.4T MRI. T_2 relaxation time was also recorded.
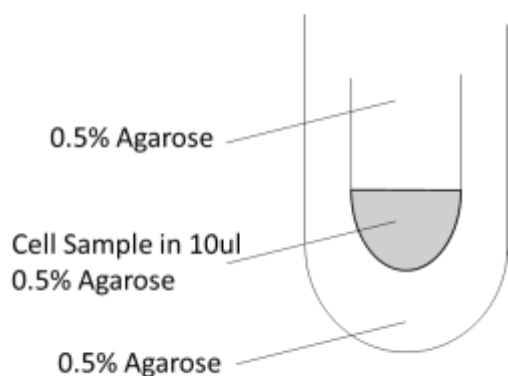
Scheme 3: Image illustrating the preparation of cell samples for MRI

0.5% Agarose

Cell Sample in 10ul
0.5% Agarose

0.5% Agarose

Cytotoxicity study

J774A.1 cells seeded into 96-well plate at a density of 5000 cells/well. After 48 h incubation, the cells were treated with different concentrations of IO@CO1 and IO@CO2 ([Ce]: 0μg/ml, 0.07μg/ml, 0.14μg/ml 0.28μg/ml, 0.56μg/ml, 1.4μg/ml, 2.8μg/ml, 5.6μg/ml, 10μg/ml, 15μg/ml, 20μg/ml). Cells were then treated with Ethodium homodimer-1 fluorescence dye to detect dead macrophages. The fluorescence intensity was measured by microplate reader Tecan X200 with excitation wavelength of 528 nm and emission wavelength of 617 nm. The fluorescence of 0μg/ml sample was determined as 100% macrophage viability. Fluorescent images and bright-field images of macrophages were also taken by Olympus IX51 fluorescence microscopy with Olympus TH4-200 visual light source and CoolLED pE-300 fluorescent light source.

In vitro ROS scavenging cell-based assay

Macrophage J774A.1 cells were seeded into 96-well plate at a density of 5000 cells/well. After 48 h incubation, cells were separately treated with different concentrations of IO@CO1 and IO@CO2 ([Ce]: 0μg/ml, 0.014μg/ml, 0.056μg/ml, 0.14μg/ml and 1.4μg/ml). After an additional 24 h incubation, macrophages were stimulated by 1.5mM H_2O_2 for 1 hour in the incubator at 37°C and 5% CO_2. Intracellular ROS levels were detected by incubating the cells with 25μM DCF_DA for 45 min in the incubator at 37°C and 5% CO_2. The fluorescence intensity was measured by Tecan X200 (ex/em: 485/535nm) and fluorescence images were

taken by Olympus IX51 fluorescence microscopy with CoolLED pE-300 fluorescent light source.

Statistical analysis of data

Data are presented as mean ± standard deviation (SD). One-way ANOVA was used in the analysis of significant difference. A p value ≤ 0.05 was considered significant. Graphs were plotted by GraphPad Prism 7.

Result and discussion

Synthesis and characterization of IO@CO nanoparticles

Recently, "core-shell nanoparticle" have attracted scientists' attention in medical areas, such as bio-modified Fe_3O_4@Au core-shell nanoparticles for targeting and multimodal imaging of cancer cells[33], Fe_3O_4@Au core-shell nanocomposites probes for the detection of mutation of DNA in aqueous solutions[34], and Fe@Fe_2O_3 core-shell nanoparticles are selectively used for the detection of damaged DNA[35]. In addition, Pt@CeO_2[36] and Au@CeO_2[37] nanocomposites were used for a better interaction in biocatalysts. In our study, an iron oxide/cerium oxide core-shell (IO@CO) nanoparticle was firstly synthesized by using reverse microemulsion approaches. TEM images (Figure 2A) showed that the IO@CO nanoparticle comprises a 10 nm Fe_3O_4 core surrounded by spherical CeO_2 nanoparticles with approximately 2 nm diameters assembling to form the shell. IO@CO1 (~55nm) was bigger than IO@CO2 (~22nm) as the central iron oxide nanocore of IO@CO1 was surrounded by more CeO_2 particles than IO@CO2. IO@CO1 and IO@CO2 had hydrodynamic sizes of 55 nm and 22 nm, respectively, with low polydispersity index (PdI) (Figure 2B). The low magnification images (Figure S1) and DLS size intensity graphs (Figure 2C) showed that IO@CO have a good distribution in water. Both of the nanoparticles were highly negatively charged.
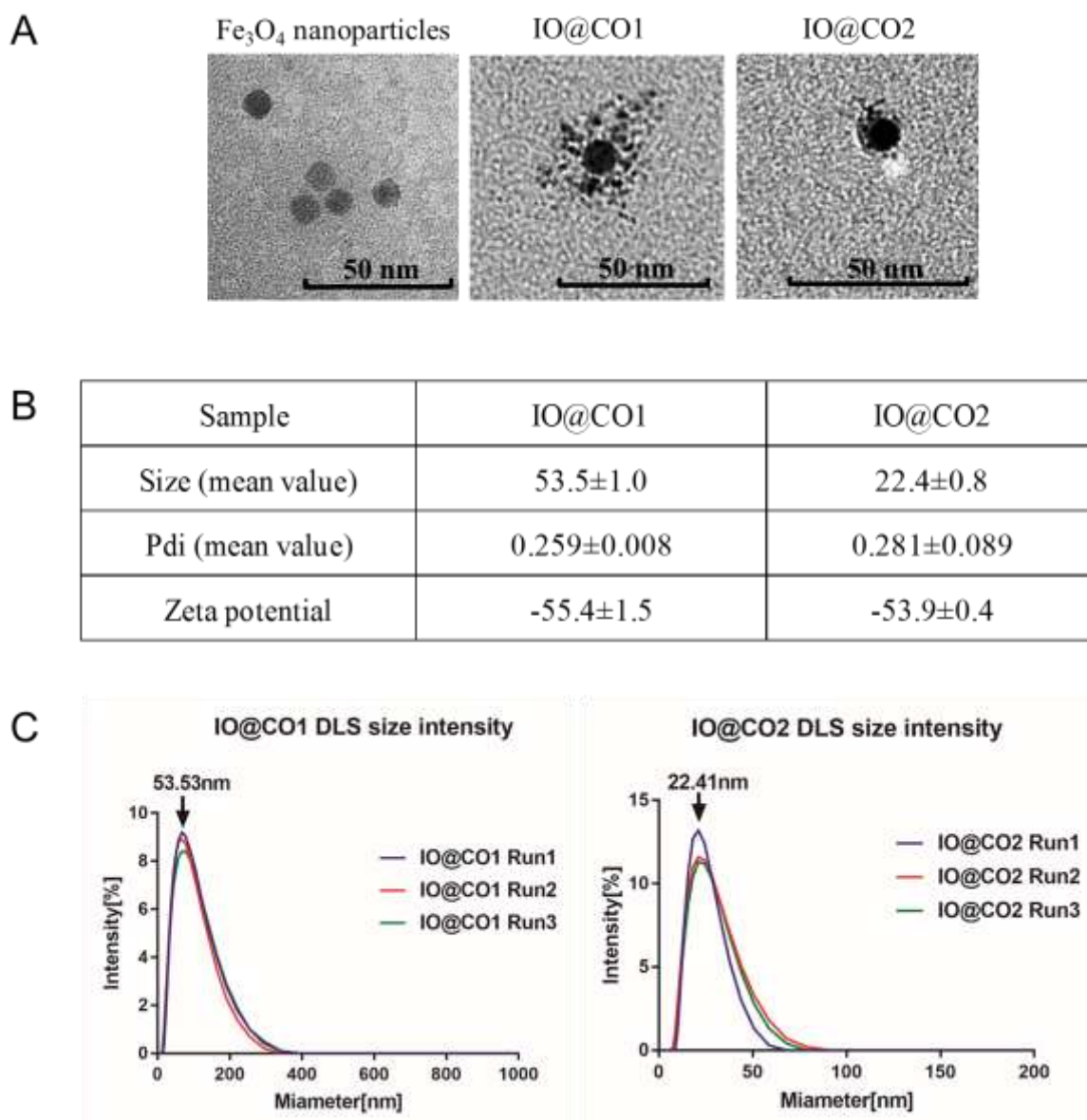
Figure 2. Characteristics of IO@CO nanoparticles. (A) TEM images of Fe_3O_4, IO@CO1 and IO@CO2 nanoparticles. IO@CO1 showed a bigger size than IO@CO2 in accordance with data from DLS Zetasizer (scale bar, 50 nm). (B) Nanoparticle size and zeta potential measured by DLS Zetasizer. Zeta potential data showed both of these two nanoparticles were negatively charged. (C) The DLS size distribution of the nanoparticles.

Fourier Transform Infrared Spectroscopy (FTIR) spectra confirmed that the peaks of chemical bonds (C-H, C=O and C-O) of PAA were shown in IO@CO nanoparticles, indicating that PAA was successfully coated on the nanoparticles (Figure 3). The carboxylic acid groups in PAA

were the key factor that links between CeO_2 and Fe_3O_4. Clusters of CeO_2 were assembled in

the presence of PAA via interfacial interaction between PAA and oxide metal surfaces. This is

the interactions between proton-donating pendent COOH groups in PAA molecules and polar

OH groups at hydrated oxide surface sites[38]. These CeO_2 clusters were then coated around

Fe_3O_4 core via the same interaction mechanism between free COOH groups on PAA molecules

and Fe_3O_4 surface. FTIR spectra IO@CO also showed a strong peak around 1500 cm-1 that

was from the iron-oleate complex. The C-O stretching at $1700cm^{-1}$ in oleic acid formed a new

peak at around $1550cm^{-1}$ after the formation of iron-carboxylate bonds[64].
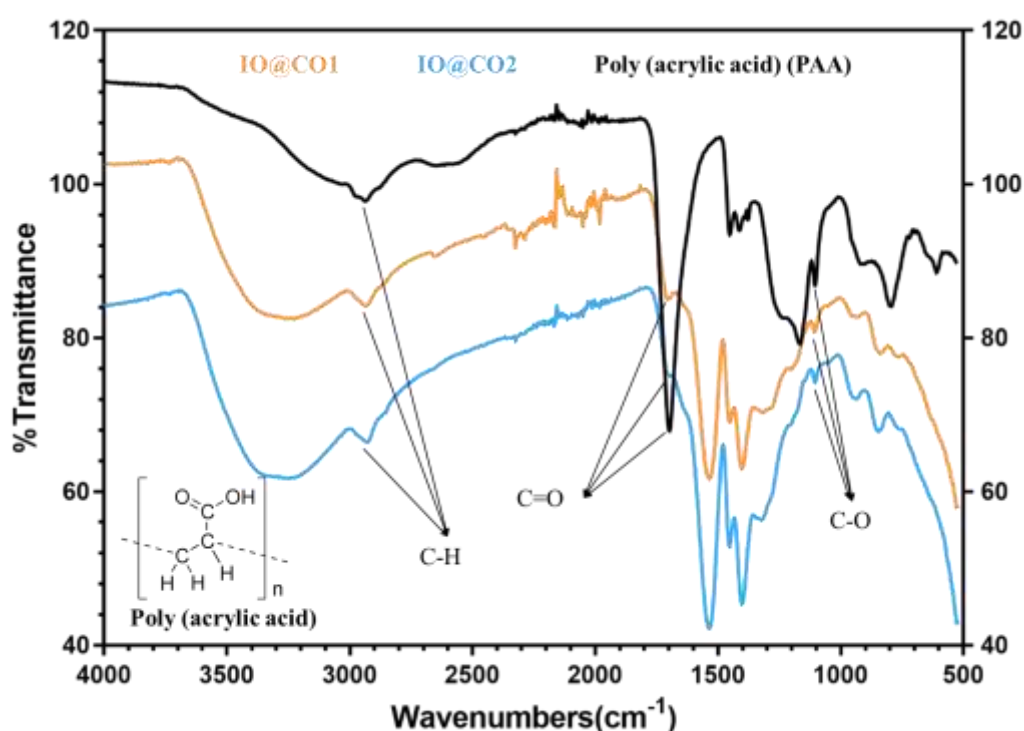
Figure 3. Infrared Spectroscopy of IO@CO nanoparticles and PAA tested by Fourier Transform Infrared Spectroscopy (FTIR). IO@CO1, IO@CO2 and PAA powders were dried followed by FTIR measurement. Three strong peaks around $2800cm^{-1}$ showed carbon-hydrogen bonds. Three peaks near $1700cm^{-1}$ indicated the existence of carbon-oxygen double bonds. Three weak peaks observed at $1150cm^{-1}$ were carbon-oxygen bands. According to PAA structure and infrared spectroscopy, PAA was successfully coated on the nanoparticles.

X-ray photoelectron spectroscopy (XPS) was employed to determine the different oxidation state of cerium that is proportional to the bioactivity of the nanoparticle. As evident from Figure 4, both trivalence cerium (Ce^{3+}) and tetravalence cerium (Ce^{4+}) oxidation states were present in nanoparticles (Figure 4A), which means these nanoparticles were able to be used for further application in ROS quenching experiment. An additional result confirmed by XPS showed that IO@CO2 had a higher ratio of Ce^{3+} to Ce^{4+} than IO@CO1 (1:3 and 1:4, respectively) (Figure 4B).
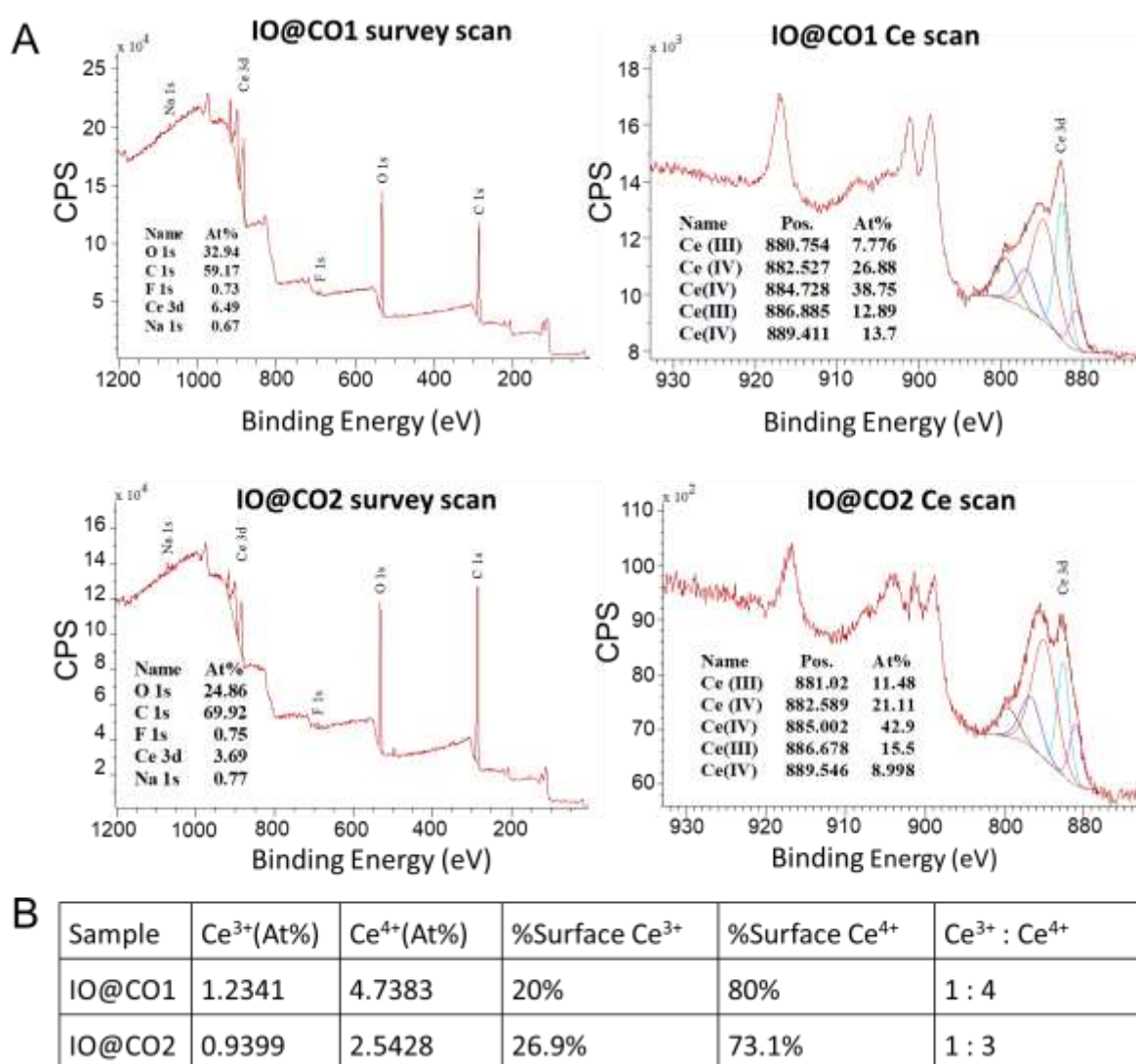

A

IO@CO1 survey scan

Name	At%
O 1s	32.94
C 1s	59.17
F 1s	0.73
Ce 3d	6.49
Na 1s	0.67

IO@CO1 Ce scan

Name	Pos.	At%
Ce (III)	880.754	7.776
Ce (IV)	882.527	26.88
Ce(IV)	884.728	38.75
Ce(III)	886.885	12.89
Ce(IV)	889.411	13.7

IO@CO2 survey scan

Name	At%
O 1s	24.86
C 1s	69.92
F 1s	0.75
Ce 3d	3.69
Na 1s	0.77

IO@CO2 Ce scan

Name	Pos.	At%
Ce (III)	881.02	11.48
Ce (IV)	882.589	21.11
Ce(IV)	885.002	42.9
Ce(III)	886.678	15.5
Ce(IV)	889.546	8.998

B

Sample	Ce^{3+}(At%)	Ce^{4+}(At%)	%Surface Ce^{3+}	%Surface Ce^{4+}	Ce^{3+} : Ce^{4+}
IO@CO1	1.2341	4.7383	20%	80%	1 : 4
IO@CO2	0.9399	2.5428	26.9%	73.1%	1 : 3

Figure 4. X-ray photoelectron spectroscopy (XPS) of IO@CO nanoparticles. Ce^{3+}: Ce^{4+} ratio is an important characteristic that relates to the antioxidant ability of the IO@CO nanoparticles. (A) The graph showing Survey

and Ce scan of IO@CO1 and IO@CO2. (B) Table showing surface Ce^{3+}, Ce^{4+}, and Ce^{3+}: Ce^{4+} ratio of IO@CO1 and IO@CO2.

Subsequently, we tested whether IO@CO nanoparticle is a good MRI contrast agent. Phantoms of IO@CO nanoparticle solutions with different iron concentrations were prepared. T_2-weighted MR images of both IO@CO1 and IO@CO2 samples were getting darker or the MRI signal of the samples decreased when the concentration of iron oxide increased. Figure 5A showed that IO@CO2 had a stronger T_2 contrast effect. Figure 5B and 5C also indicated that IO@CO2 had a higher T_2-weighted relaxivity (r_2) than IO@CO1 (378 and 339 mM^{-1}, s^{-1}, respectively). IO@CO2 showed a steeper slope of relaxation rate than IO@CO1, which could result from the thinner surrounding CeO_2 layer. However, both IO@CO1 and IO@CO2 are good contrast agents and can be used in further *in vitro* MRI studies.
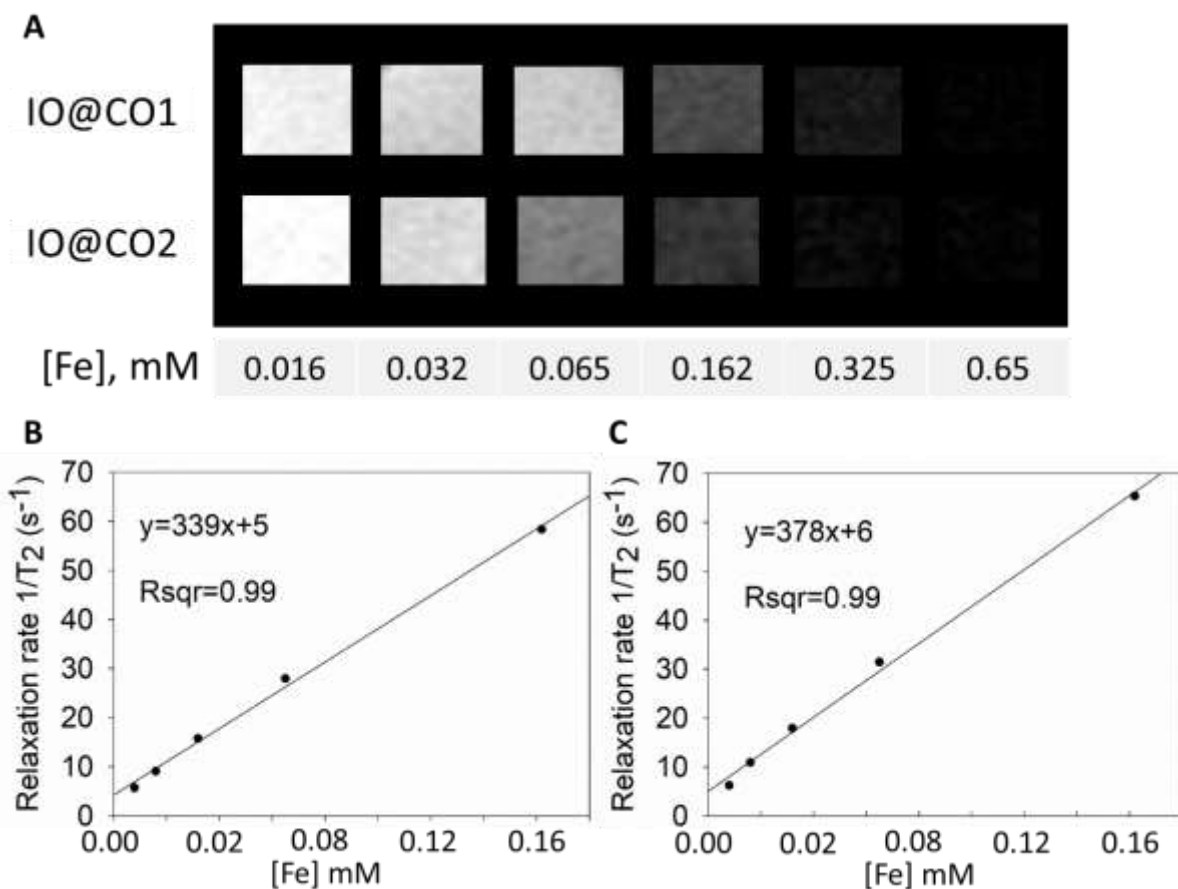
Figure 5. MRI of IO@CO nanoparticle phantoms. (A) MRI images of IO@CO1 & IO@CO2 phantoms. IO@CO1 and IO@CO2 were diluted to different concentrations followed by imaging using 9.4T MRI. (B) Graph plotting the relationship of relaxation rate and iron concentration of IO@CO1. (C) Graph plotting the relationship of relaxation rate and iron concentration of IO@CO2.

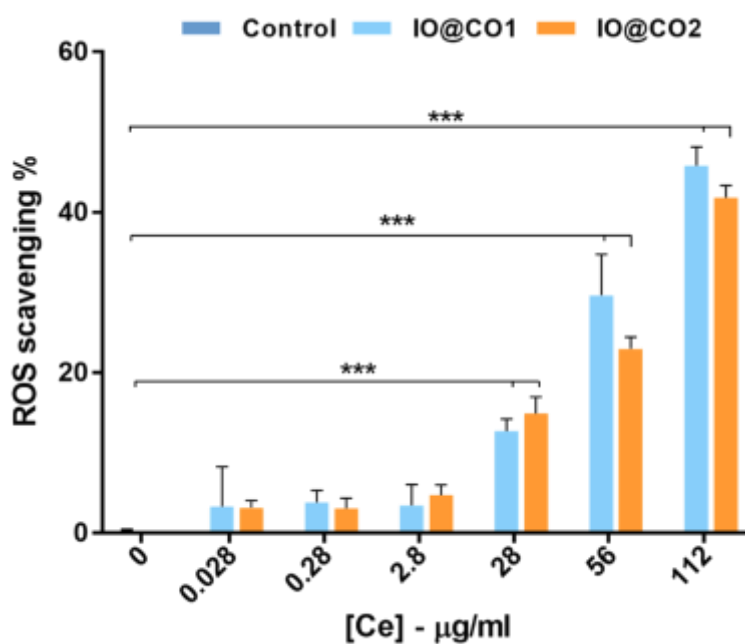## *ROS scavenging capability of IO@CO nanoparticles*

Figure 6. ROS scavenging study of IO@CO nanoparticles. Different concentrations of the nanoparticles were treated with H_2O_2 followed by HRP treatment. Then ABTS was added into each reaction and absorbance was measured by Tecan X200. The absorbance of 0μg/ml sample was determined as 0% ROS scavenging. ***P<0.001.

Previous studies illustrated that cerium oxide nanoparticles had catalase mimetic activity, and were able to reduce the level of hydrogen peroxide H_2O_2 [39]. Here we investigated whether our IO@CO nanoparticles have ROS scavenging ability. We use the H_2O_2-HRP-ABTS system to test the anti-ROS capability of the nanoparticles. Briefly, ABTS (2,2'-azino-bis(3-ethylbenzothiazoline-6-sulphonic acid) was oxidized by hydrogen peroxide (H_2O_2) in the presence of horseradish peroxidase (HRP) as a catalyst. As mentioned previously, cerium oxide can scavenge both H_2O_2 and superoxide radical when the cerium oxidation state changes between tervalence and tetravalence. Therefore, we incubated our nanoparticles with hydrogen

peroxide followed by adding HRP. Finally, ABTS was added to detect ROS. We observed a significant decrease in absorbance (directly proportional to ROS level) when the concentration of cerium increased to 280ng/100µl and above (Figure 6). Moreover, the nanoparticles with Ce concentration of 1120ng/100µl were able to scavenge nearly half of the ROS in the solution. Our result showed that IO@CO nanoparticles have anti-ROS ability in the buffer solution.
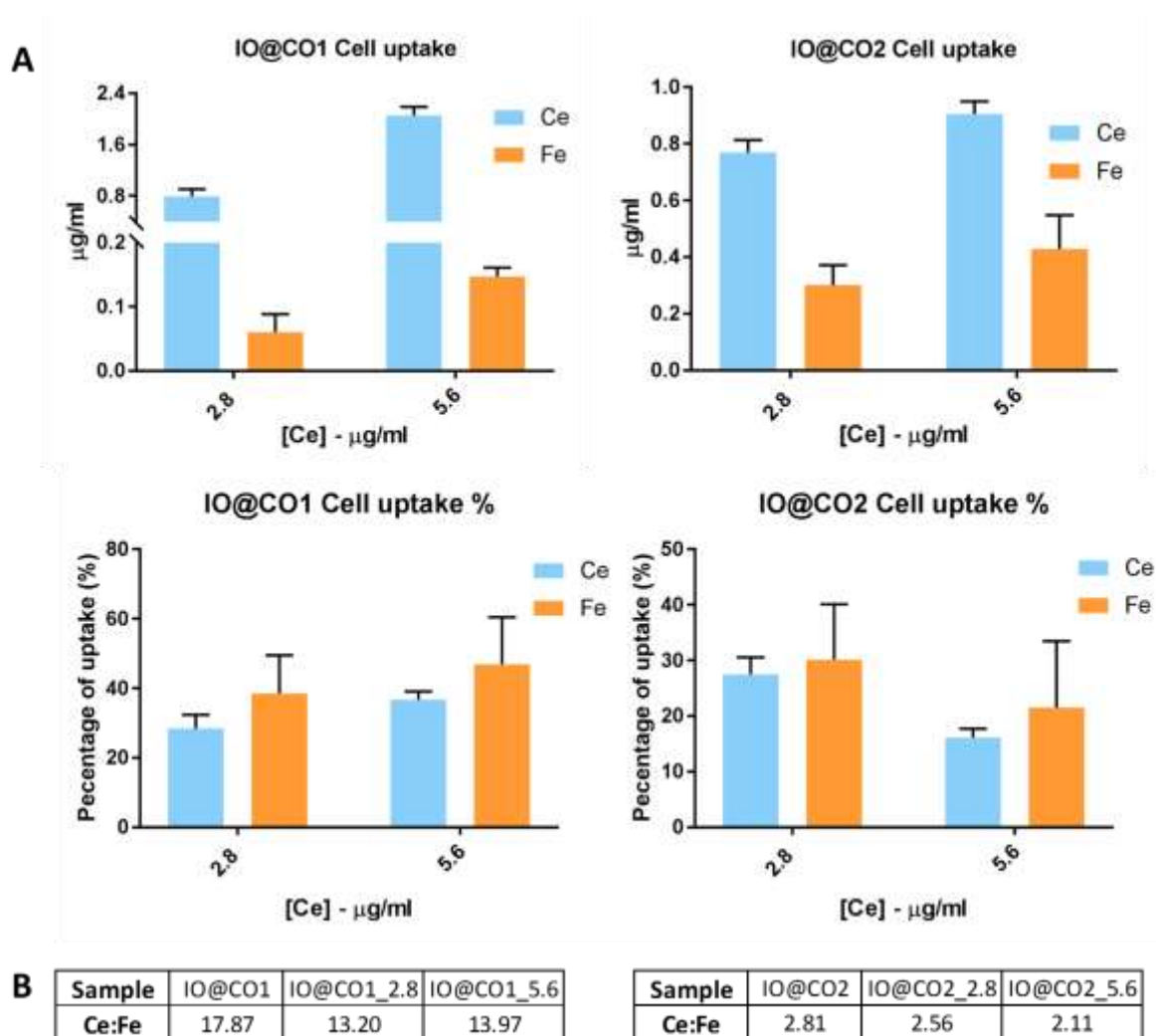
Nanoparticle uptake in macrophage J774A-1

Sample	IO@CO1	IO@CO1_2.8	IO@CO1_5.6
Ce:Fe	17.87	13.20	13.97

Sample	IO@CO2	IO@CO2_2.8	IO@CO2_5.6
Ce:Fe	2.81	2.56	2.11

Figure 7. Cell uptake of IO@CO nanoparticles as determined by ICP-MS. (A) Graphs showing cell uptake of IO@CO. Macrophage cells were incubated with IO@CO nanoparticles overnight. The cells were subsequently lysed. Iron and cerium concentrations were detected by ICP-MS. The graphs showed that both IO@CO1 and IO@CO2 were uptaken by macrophages. (B) Tables showing ratios of cerium to iron in the nanoparticle stocks and in cells.

Before conducting the *in vitro* cell-based studies, we sought to determine the macrophage uptake of these nanoparticles to make sure our nanoparticles can work inside the cells. Macrophages were used for our *in vitro* experiments as they are the cells responsible for ROS production in inflammatory conditions.[5, 12] Macrophages were treated with the nanoparticles of different concentrations. The cells were washed and lysed, followed by measuring the cerium and iron concentration in the cell lysis buffer.

ICP-MS measurement (Figure 7) demonstrated that our nanoparticles had good macrophage uptake. The results from both cerium and iron uptake in the cells indicated that these IO@CO nanoparticles were successfully entered into the macrophage cells with considerable quantity. When treated with higher concentrations of the nanoparticles, both cerium and iron uptake in macrophages significantly increased. The ratios of Ce to Fe uptaken by the cells were compared with the ratios of Ce to Fe in the nanoparticles (Figure 7B). For IO@CO1, the ratios in the cells were detected lower than the ratio in the nanoparticle. For IO@CO2, the ratios in the cells slightly less than the ratio in the nanoparticle. The decrease of the Ce/Fe ratio could be explained by the loss of cerium oxide in IO@CO nanoparticles due to nanoparticle degradation at low pH within the lysosome environment. Our degradation studies (Supporting Information Figure S2) showed that the size of IO@CO nanoparticles slightly decreased at acidic pH condition (pH5.5). This could be explained by the shrinkage of poly(acrylic acid) at low pH environment due to the protonation of carboxylic groups[65]. The reduced size of the nanoparticles could also be contributed by the dissolution of cerium oxide in acidic condition[66]. The reason why IO@CO1 exhibited larger decrease in Ce/Fe ratio in the cell, compared to IO@CO2, is unclear but may be due to the higher loading of CeO_2 on IO@CO2, leading to a more pronounced change of Ce/Fe ratios when CeO_2 is degraded.

It was noted that the IO@CO nanoparticles were highly negatively charged (-55 mV) but able to be taken by the cells. This can be explain as following. Basically, the cell membranes should repulse the negatively charged IO@CO because of the large amount of negatively charged domains on their surface. However, Wilhelm et al.[60] indicated that with a repulsive force from the negatively charged domains on the surface of the membranes, the negatively charged nanoparticles will form into small groups then bind at the cationic sites on the surface. Meanwhile, the existing nanoparticles on the cell surface can reduce the density of the surface charge, which will benefit the adsorption of other nanoparticles. Therefore, the process of adsorption of the nanoparticles on the cell surface and the formation of the particle clusters are related to their cell uptake. Studies by Limbach et al. and Patil st al. on human lung cells also indicated that cells rapidly absorb negatively charged ceria nanoparticles[61-62]. In addition, Tabata et al. suggested that the lowest uptake of the nanoparticles in macrophages are related to surface charge with a zeta potential of zero. In their study, negatively charged cell membranes along with the cations in the cell culture medium such as Ca2+ and Mg2+ were closely related to the cell uptake of both of their positively and negatively charged microspheres[63].

In vitro magnetic resonance imaging of IO@CO nanoparticle in macrophages

In the last decades, SPIONs have been widely studied for imaging technology. For example, Fong-Yu et al. indicated that aqueous dispersions of Fe_3O_4 nanoparticles had excellent ability of imaging in the cell with low cytotoxicity.[40] Ta et al has developed different iron oxide nanoparticles for molecular MR imaging of cardiovascular diseases such as atherothrombosis[41-46]. After confirming IO@CO nanoparticles were good contrast agents, we investigated the contrast ability of the nanoparticles inside macrophage J774A.1. Cells were incubated for 24h with nanoparticles and subsequently fixed by paraformaldehyde. Then the cell pellet was embedded in the 0.5% agarose gel followed by MRI measurement.

The relaxation rates (Figure 8A) and MR images (Figure 8B) of the nanoparticle-treated cells had a considerable enhancement than those without nanoparticle. Especially IO@CO2 had much stronger MRI T_2 effect and a higher relaxation rate than IO@CO1. The stronger T_2 contrast effect of IO@CO2 could result from its higher iron uptake as shown in cell uptake study. These results showed that both IO@CO1 and IO@CO2 were able to image macrophage cells; especially IO@CO2 had a more significant imaging contrast effect.
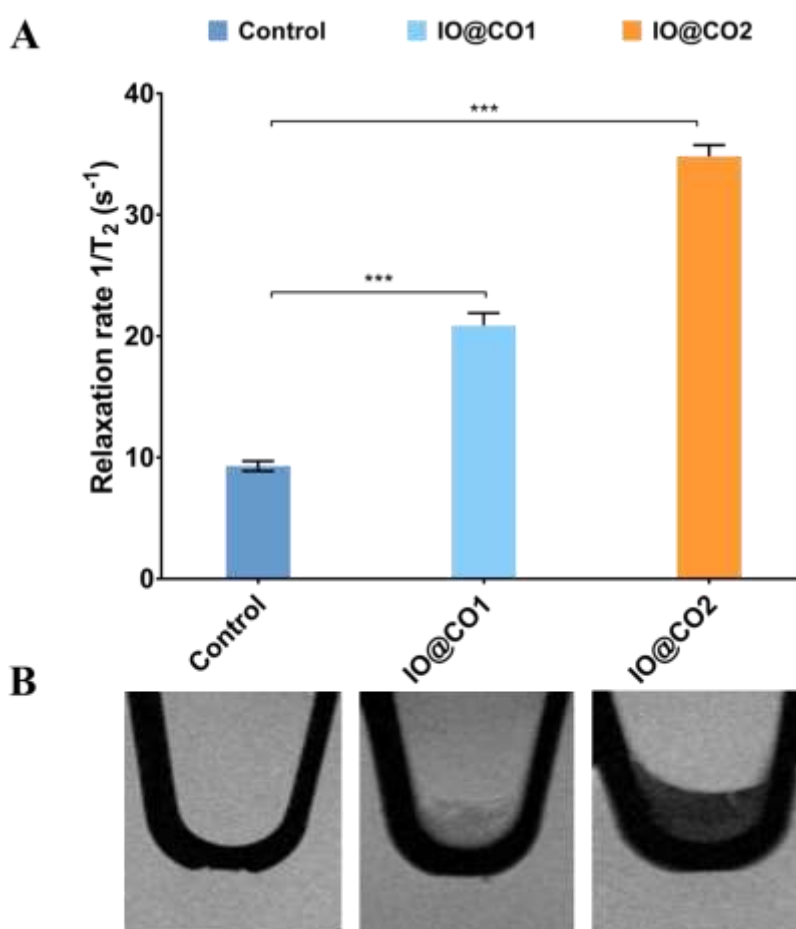

Figure 8. In vitro MRI of IO@CO nanoparticles. Macrophage cells were incubated with IO@CO nanoparticles overnight. The cells were subsequently fixed, suspended in 0.5% agarose gel and imaged by MRI. (A) Graph showing relaxation rate of the non-treated cells, and cells treated with IO@CO1 and IO@CO2. The relaxation rate of the nanoparticle-treated sample is higher than non-treated group (Control). (B) MRI images of the cells. Both CO@IO1 & CO@IO2 nanoparticle-treated samples had significant imaging signal (dark color) than non-treated group (control). In addition, cells incubated with IO@CO2 had the stronger negative MRI effect than the cells incubated with IO@CO1. ***$P<0.001$.

Biocompatibility of IO@CO nanoparticles

Before testing the ROS quenching ability of IO@CO nanoparticle in the cells, it is necessary to investigate cytotoxic effect of these nanoparticles, even though it was reported that cerium oxide nanoparticles had no toxic effect on macrophage cells.[49] Macrophages J774A.1 (20,000 cells per well) were used to test the cytotoxic effect of the nanoparticles and were treated with different concentrations of nanoparticles for 24 hours and 48 hours. Cells were then washed and subsequently treated with EthD-1 that marked the dead macrophage nucleus and can be detected by its red fluorescence. Cells were imaged by fluorescence microscopy (Figure 9B) and fluorescence intensity was measured by plate reader (Figure 9A). There was no significant difference between live cell control and nanoparticle-treated groups. Fluorescence images also indicated a low cytotoxicity of the nanoparticles after 24-hour treatment. In two-day treatment, macrophages treated with IO@CO2 still showed very good cell viability. However, we observed a slight decrease in the viability of macrophages treated with high concentrations of IO@CO1. The result indicated that IO@CO1 had some toxic effects on macrophage cells, while IO@CO2 had no cytotoxic effect in any concentrations and time periods tested in the study.
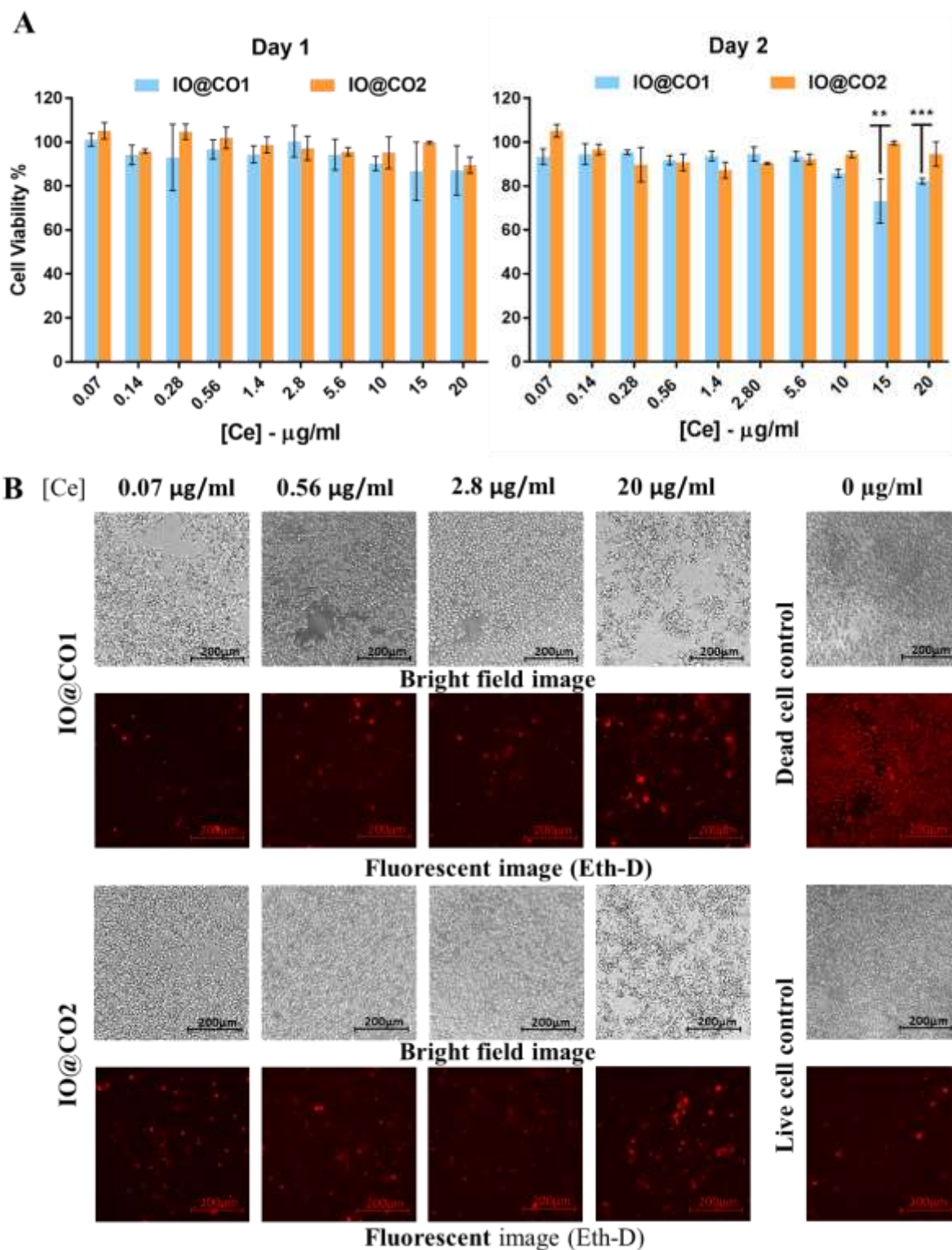
Figure 9. Viability/toxicity study of macrophage cells with nanoparticles. Macrophage cells were incubated with IO@CO nanoparticles for one or two days. Dead cells were stained by EthD-1 and showed the red fluorescence under fluorescence microscopy. The fluorescence intensity was measured by Tecan X200. (A) Graph

showing the viability of the cells after one- or two-day incubation with the nanoparticles. It showed that cell viability was around 90%-100% for all different concentrations of nanoparticles, except the cells that were treated with IO@CO1 in very high concentrations. These cells showed approximately 70-80% of viability of cells. (B) Fluorescence images of the cells taken on the first day of the nanoparticle treatment. It showed that the toxicity of IO@CO nanoparticles was acceptable. **$P<0.01$, ***$P<0.001$.

In vitro cell-based assay of ROS scavenging capability

Reactive oxygen species have been related to a broad spectrum of inflammatory diseases such as atherosclerosis and rheumatoid arthritis. In this decade, cerium oxide nanoparticles have been confidently shown to have the ROS scavenging capability *in vitro*. David et al. in 2006 firstly showed that cerium oxide nanoparticle (with Ce^{3+}: Ce^{4+} ratio of 3:47) could protect rat hippocampal nerve cell from hydrogen peroxide-induced cell death effectively[50] and it also worked on human breast fibrosarcoma cell[51]. In addition, in 2009 Suzanne et al. showed cerium oxide nanoparticle could reduce ROS in macrophage J774A.1 cells significantly.[49]

In our studies, we chose to use macrophage as our cell model as it has been reported as a major factor in many inflammatory diseases[52-54]. Due to higher toxicity of IO@CO1, IO@CO2 was chosen for *in vitro* cell-based assay of ROS scavenging effect. Macrophages were incubated for 24 hours with different concentrations of nanoparticles and subsequently stimulated by 1.5mM H_2O_2. After that, dichlorofluorescin diacetate (DCF_DA) was used to detect ROS levels in the cells. H_2O_2 is the most studied and best-characterized member of ROS and it can be regarded as the most important ROS in redox signaling. The fluorescence intensity (Figure 10A) showed that compared to H_2O_2 treated control group, the ROS level of the cells treated with 0.056 μg Ce/ml was significantly decreased. When Ce concentration rose to 0.14 μg/ml and above, the ROS level of the treated cells was lowered to the ROS level of the control non-stimulated cells. Fluorescence images (Figure 10B) of nanoparticle-treated macrophages showed a similar fluorescence signal with non-stimulated cell control group and significantly

weaker than the stimulated cell control group. These results confirmed the ROS scavenging ability of our IO@CO2 *in vitro*.
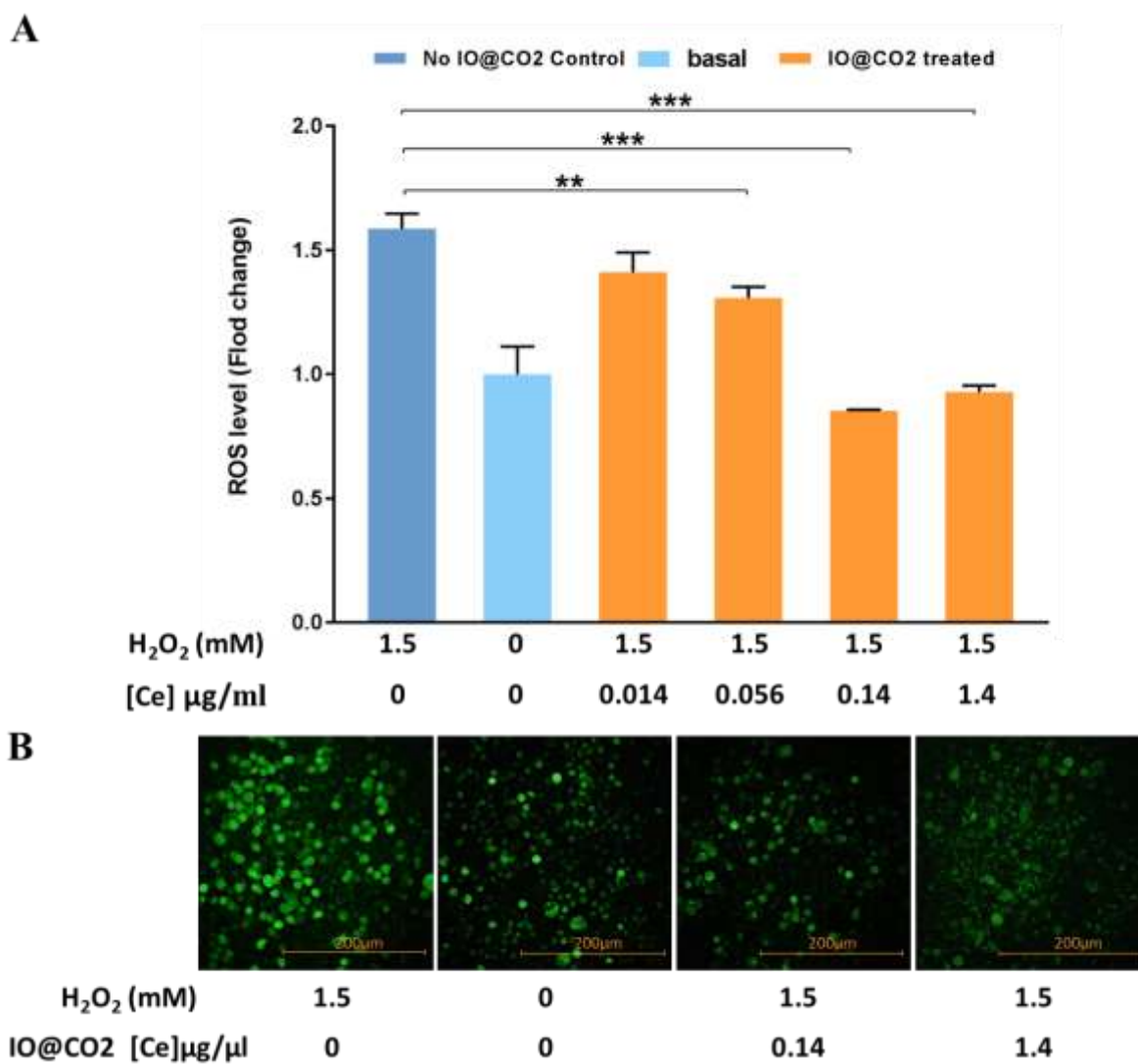

Figure 10. ROS scavenging ability of IO@CO nanoparticles in macrophage cells. Macrophage cells were incubated with IO@CO nanoparticles overnight followed by stimulated by H_2O_2. ROS inside the cells were detected by DCF_DA. The fluorescence intensity was measured by Tecan X200 and fluorescence images were taken by fluorescence microscopy. (A) Graph showing ROS level of the cells. Cells treated with low concentration of nanoparticles showed a significant reduction of ROS when the concentration of cerium reached 14ng/100ul and above. (B) Fluorescence images of the cells. The images showed that cells treated with different concentration of nanoparticles and H_2O_2 had significant lower green fluorescence signal than the cells treated with H_2O_2. **P<0.01, ***P<0.001.

Atherosclerosis, rheumatoid arthritis, allergies and other autoimmune diseases are basically caused by chronic inflammation, which relates to disorder of inflammatory regulation or switching off.[5] These inflammatory disorders have a strong relationship with the high level of ROS in the lesions.[6, 55] For example, atherosclerosis, taking the largest proportion in the CVDs, is a complex disease that happens in the intima of arteries and can be progressive for many years[14]. In the progression of atherosclerosis, ROS plays an important role in the oxidation of low-density lipoprotein in the intima of the blood vessel by macrophage[56]. High level of the ROS along with the cytokines released by dead macrophage attracts more macrophage to accumulate into the atherosclerosis plaque, making the situation worse.[48] Similarly, in many joint diseases, ROS and NO along with some pro-inflammatory factors such as prostaglandins and cytokines are produced at sites of inflammation and are responsible for the progression of the diseases.[57]

Our result (Figure 6) showed that IO@CO had good anti-ROS ability in the buffer solution. *In vitro* cell-based ROS scavenging results (Figure 10) indicated that IO@CO2 could reduce the ROS level in macrophage cells, implying that this nanoparticle can be a potential treatment agent for inflammatory diseases such as cardiovascular disease and rheumatoid arthritis. The anti-ROS capability could be due to the regenerative antioxidant property from cerium oxide[58]. When the trivalent cerium ions change to tetravalent cerium ions, cerium ions are capable of scavenging superoxide radical. On the contrary, when it comes back from tetravalent cerium ions to trivalent cerium ions, cerium ions show the ability of scavenging H_2O_2. These regenerative antioxidant capabilities are the major reasons that IO@CO nanoparticles can reduce the ROS level in macrophage cells. Janet et al. recently showed that changing of $Ce^{3+}:Ce^{4+}$ ratio on the nanoparticle surface can alter the biological interactions of the nanoparticle.[59] In addition, it is shown that 22% of Ce^{3+} atom on the surface of nanoparticles

will significantly contribute stronger activities of superoxide dismutase [19]. In our study, the reliable antioxidant activity of the IO@CO nanoparticles owned to the ideal concentration of Ce^{3+} atom (20% and 26.9%) on their surface, which contribute the good ROS scavenging ability of these IO@CO nanoparticles. In Bae et al. study[67], they developed hydrogen peroxide-responsive antioxidant copolyoxalates containing hydroxybenzyl alcohol (HPOX) and vanillyl alcohol (PVAX) nanoparticles , which showed a good H_2O_2 scavenging ability around 40% to 60% after 24 hours treated with 1mg/ml of their nanoparticle. IO@CO has a good anti-H_2O_2 ability at 50% after only 1 hour treated with just 112µg/ml of cerium oxide of IO@CO. In *in vitro* cell study, IO@CO2 showed more than 50% scavenge of ROS at 0.14µg/ml and 1.4µg/ml of cerium oxide of IO@CO2. In Liu et al[68] study, the ROS scavenging ability of 1µM nano-CeO_2 (12 hour treatment) was around 20% in HepG2 cells that exposed to 0.6 mM H_2O_2 for 12 hours. In our study, macrophage J774.A1 was treated with IO@CO2 for 24 hours followed by 1 hour incubation with 1.5mM H_2O_2. It showed a good the ROS scavenging around 73% when the cerium concentration of IO@CO2 was 0.14µg/ml.

Conclusion

The presented data demonstrate a successful synthesis of iron oxide/cerium oxide core-shell (IO@CO) nanoparticle. IO@CO nanoparticles were shown to be a good contrast agent under MRI, and they also exhibited a good $Ce^{3+}:Ce^{4+}$ ratio. *In vitro* studies showed that our nanoparticles had good cell uptake, strong cell MRI, low cell cytotoxicity and good ROS scavenging ability. The results showed that IO@CO nanoparticle could decrease ROS level in the stimulated J774A.1 macrophages. The ROS scavenging ability of IO@CO in macrophage makes this nanoparticle a potential treatment agent for ROS-related inflammatory diseases such as atherosclerosis and rheumatoid arthritis. In addition, good MRI imaging capability of the nanoparticle indicates its potential use for detecting and monitoring the treatment of inflammatory diseases. In conclusion, IO@CO nanoparticles can be a potential theranostic

agent for inflammatory diseases. In the future, we will conjugate our nanoparticle with antibodies or binding peptides to target inflammatory markers. For example, vascular cell adhesion molecule 1 (VCAM-1) is one of the important adhesion molecules secreted by the inflamed endothelial cells especially those in atherosclerotic plaques[47]. Therefore, VCAM-1 is an effective biomarker to detect endothelial inflammation, improving the progress for both early phase treatment and early stage detection of atherosclerosis and CVD. In rheumatoid arthritis, Neutrophil Cytosolic Factor 1 can be a good biomarker of RA as it is highly expressed in the inflammatory position of the rheumatoid arthritis patient.[48] By employing an effective targeting ligands, these nanoparticles can detect the early stage of atherosclerosis, rheumatoid arthritis and other ROS related inflammatory diseases. In addition, further studies on the applications of these nanoparticles in animal models of inflammatory diseases will be conducted in the future.

Conflicts of interest

Nothing to declare.

Acknowledgement

References

1.   S. Barquera, A. Pedroza-Tobias, C. Medina, L. Hernandez-Barrera, K. Bibbins-Domingo, R. Lozano and A. E. Moran, *Arch Med Res*, 2015, **46**, 328-338.

2.   M. Naghavi, H. D. Wang, R. Lozano, A. Davis, X. F. Liang, M. G. Zhou, S. E. Vollset, A. A. Ozgoren, S. Abdalla, F. Abd-Allah, M. I. A. Aziz, S. F. Abera, V. Aboyans, B. Abraham, J. P. Abraham, K. E. Abuabara, I. Abubakar, L. J. Abu-Raddad, N. M. E. Abu-Rmeileh, T. Achoki, A. Adelekan, Z. N. Ademi, K. Adofo, A. K. Adou, J. C. Adsuar, J. Aernlov, E. E. Agardh, D. Akena, M. J. Al Khabouri, D. Alasfoor, M. Albittar, M. A. Alegretti, A. V. Aleman, Z. A. Alemu, R. Alfonso-Cristancho, S. Alhabib, M. K. Ali, R. Ali, F. Alla, F. Al Lami, P. Allebeck, M. A. AlMazroa, R. A. S. Salman, U. Alsharif, E. Alvarez, N. Alviz-Guzman, A. A. Amankwaa, A. T. Amare, O. Ameli, H. Amini, W. Ammar, H. R. Anderson, B. O. Anderson, C. A. T. Antonio, P. Anwari, H. Apfel, S. A. Cunningham, V. S. A. Arsenijevic, A. Artaman, M. M. Asad, R. J. Asghar, R. Assadi, L. S. Atkins, C. Atkinson, A. Badawi, M. C. Bahit, T. Bakfalouni, K. Balakrishnan, S. Balalla, A. Banerjee, R. M. Barber, S. L. Barker-Collo, S. Barquera, L. Barregard, L. H. Barrero, T. Barrientos-Gutierrez, A. Basu, S. Basu, M. O. Basulaiman, J. Beardsley, N. Bedi, E. Beghi, T. Bekele, M. L. Bell, C. Benjet, D. A. Bennett, I. M. Bensenor, H. Benzian, A. Bertozzi-Villa, T. J. Beyene, N. Bhala, A. Bhalla, Z. A. Bhutta, B. Bikbov, A. Bin Abdulhak, S. Biryukov, J. D. Blore, F. M. Blyth, M. A. Bohensky, G. Borges, D. Bose, S. Boufous, R. R. Bourne, L. N. Boyers, M. Brainin, M. Brauer, C. E. G. Brayne, A. Brazinova, N. Breitborde, H. Brenner, A. D. M. Briggs, J. C. Brown, T. S. Brugha, G. C. Buckle, L. N. Bui, G. Bukhman, M. Burch, I. R. C. Nonato, H. Carabin, R. Cardenas, J. Carapetis, D. O. Carpenter, V. Caso, C. A. Castaneda-Orjuela, R. E. Castro, F. Catala-Lopez, F. Cavalleri, J. C. Chang, F. C. Charlson, X. Che, H. L. Chen, Y. Y. Chen, J. S. Chen, Z. M. Chen, P. P. C. Chiang, O. Chimed-Ochir, R. Chowdhury, H. Christensen, C. A. Christophi, T. W. Chuang, S. S. Chugh, M. Cirillo, M. M. Coates, L. E. Coffeng, M. S. Coggeshall, A. Cohen, V. Colistro, S. M. Colquhoun, M. Colomar, L. T. Cooper, C. Cooper, L. M. Coppola, M. Cortinovis, K. Courville, B. C. Cowie, M. H. Criqui, J. A. Crump, L. Cuevas-Nasu, I. D. C. Leite, K. C. Dabhadkar, L. Dandona, R. Dandona, E. Dansereau, P. I. Dargan, A. Dayama, V. De la Cruz-Gongora, S. F. de la Vega, D. De Leo, L. Degenhardt, B. del Pozo-Cruz, R. P. Dellavalle, K. Deribe, D. C. D. Jarlais, M. Dessalegn, G. A. deVeber, S. D. Dharmaratne, M. Dherani, J. L. Diaz-Ortega, C. Diaz-Torne, D. Dicker, E. L. Ding, K. Dokova, E. R. Dorsey, T. R. Driscoll, L. L. Duan, H. C. Duber, A. M. Durrani, B. E. Ebel, K. M. Edmond, R. G. Ellenbogen, Y. Elshrek, S. P. Ermakov, H. E. Erskine, B. Eshrati, A. Esteghamati, K. Estep, T. Furst, S. Fahimi, A. S. Fahrion, E. J. A. Faraon, F. Farzadfar, D. F. J. Fay, A. B. Feigl, V. L. Feigin, M. M. Felicio, S. M. Fereshtehnejad, J. G. Fernandes, A. J. Ferrari, T. D. Fleming, N. Foigt, K. Foreman, M. H. Forouzanfar, F. G. R. Fowkes, U. F. Paleo, R. C. Franklin, N. D. Futran, L. Gaffikin, K. Gambashidze, F. G. Gankpe, F. A. Garcia-Guerra, A. C. Garcia, J. M. Geleijnse, B. D. Gessner, K. B. Gibney, R. F. Gillum, S. Gilmour, I. Abdelmageem, M. Ginawi, M. Giroud, E. L. Glaser, S. Goenka, H. G. Dantes, P. Gona, D. Gonzalez-Medina, C. Guinovart, R. Gupta, R. Gupta, R. A. Gosselin, C. C. Gotay, A. Goto, H. N. Gowda, N. Graetz, K. F. Greenwell, H. C. Gugnani, D. Gunnell, R. A. Gutierrez, J. Haagsma, N. Hafezi-Nejad, H. Hagan, M. Hagstromer, Y. A. Halasa, R. R. Hamadeh, H. Hamavid, M. Hammami, J. Hancock, G. J. Hankey, G. M. Hansen, H. L. Harb, H. Harewood, J. M. Haro, R. Havmoeller, R. J. Hay, S. I. Hay, M. T. Hedayati, I. B. H. Pi, K. R. Heuton, P. Heydarpour, H. Higashi, M. Hijar, H. W. Hoek, H. J. Hoffman, J. C. Hornberger, H. D. Hosgood, M. Hossain, P. J. Hotez, D. G. Hoy, M. Hsairi, G. Q. Hu, J. J. Huang, M. D. Huffman, A. J. Hughes, A. Husseini, C. Huynh, M. Iannarone, K. M. Iburg, B. T. Idrisov, N. Ikeda, K. Innos, M. Inoue, F. Islami, S. Ismayilova, K. H. Jacobsen, S. Jassal, S. P. Jayaraman, P. N. Jensen, V. Jha, G. H. Jiang, Y. Jiang, J. B. Jonas, J. Joseph, K. Juel, E. K. Kabagambe, H. D. Kan, A. Karch, C. Karimkhani, G. Karthikeyan, N. Kassebaum, A. Kaul, N. Kawakami, K. Kazanjan, D. S. Kazi, A. H. Kemp, A. P. Kengne, A. Keren, M. Kereselidze, Y. S.

Khader, S. E. A. H. Khalifa, E. A. Khan, G. Khan, Y. H. Khang, C. Kieling, Y. Kinfu, J. M. Kinge, D. Kim, S. Kim, M. Kivipelto, L. Knibbs, A. K. Knudsen, Y. Kokubo, S. Kosen, M. Kotagal, M. A. Kravchenko, S. Krishnaswami, H. Krueger, B. K. Defo, E. J. Kuipers, B. K. Bicer, C. Kulkarni, V. S. Kulkarni, K. Kumar, R. B. Kumar, G. F. Kwan, H. Kyu, T. Lai, A. L. Balaji, R. Lalloo, T. Lallukka, H. Lam, Q. Lan, V. C. Lansingh, H. J. Larson, A. Larsson, P. M. Lavados, A. E. B. Lawrynowicz, J. L. Leasher, J. T. Lee, J. Leigh, M. Leinsalu, R. Leung, C. Levitz, B. Li, Y. C. Li, Y. M. Li, C. Liddell, S. S. Lim, G. M. F. de Lima, M. L. Lind, S. E. Lipshultz, S. W. Liu, Y. Liu, B. K. Lloyd, K. T. Lofgren, G. Logroscino, S. J. London, J. Lortet-Tieulent, P. A. Lotufo, R. M. Lucas, R. Lunevicius, R. A. Lyons, S. Ma, V. M. P. Machado, M. F. MacIntyre, M. T. Mackay, J. H. MacLachlan, C. Magis-Rodriguez, A. A. Mahdi, M. Majdan, R. Malekzadeh, S. Mangalam, C. C. Mapoma, M. Marape, W. Marcenes, C. Margono, G. B. Marks, M. B. Marzan, J. R. Masci, M. T. Q. Mashal, F. Masiye, A. J. Mason-Jones, R. Matzopolous, B. M. Mayosi, T. T. Mazorodze, J. J. McGrath, A. C. Mckay, M. Mckee, A. McLain, P. A. Meaney, M. M. Mehndiratta, F. Mejia-Rodriguez, Y. A. Melaku, M. Meltzer, Z. A. Memish, W. Mendoza, G. A. Mensah, A. Meretoja, F. A. Mhimbira, T. R. Miller, E. J. Mills, A. Misganaw, S. K. Mishra, C. N. Mock, T. E. Moffitt, N. M. Ibrahim, K. A. Mohammad, A. H. Mokdad, G. L. Mola, L. Monasta, J. D. Monis, J. C. M. Hernandez, M. Montico, T. J. Montine, M. D. Mooney, A. R. Moore, M. Moradi-Lakeh, A. E. Moran, R. Mori, J. Moschandreas, W. N. Moturi, M. L. Moyer, D. Mozaffarian, U. O. Mueller, M. Mukaigawara, E. C. Mullany, J. Murray, A. Mustapha, P. Naghavi, A. Naheed, K. S. Naidoo, L. Naldi, D. Nand, V. Nangia, K. M. V. Narayan, D. Nash, J. Nasher, C. Nejjari, R. G. Nelson, M. Neuhouser, S. P. Neupane, P. A. Newcomb, L. Newman, C. R. Newton, M. Ng, F. N. Ngalesoni, G. Nguyen, N. T. T. Nguyen, M. I. Nisar, S. Nolte, O. F. Norheim, R. E. Norman, B. Norrving, L. Nyakarahuka, S. Odell, M. O'Donnell, T. Ohkubo, S. L. Ohno, B. O. Olusanya, S. B. Omer, J. N. Opio, O. E. Orisakwe, K. F. Ortblad, A. Ortiz, M. L. K. Otayza, A. W. Pain, J. D. Pandian, C. I. Panelo, J. Panniyammakal, C. Papachristou, A. J. P. Caicedo, S. B. Patten, G. C. Patton, V. K. Paul, B. Pavlin, N. Pearce, C. A. Pellegrini, D. M. Pereira, S. C. Peresson, R. Perez-Padilla, F. P. Perez-Ruiz, N. Perico, A. Pervaiz, K. Pesudovs, C. B. Peterson, M. Petzold, B. K. Phillips, D. E. Phillips, M. R. Phillips, D. Plass, F. B. Piel, D. Poenaru, S. Polinder, S. Popova, R. G. Poulton, F. Pourmalek, D. Prabhakaran, D. Qato, A. D. Quezada, D. A. Quistberg, F. Rabito, A. Rafay, K. Rahimi, V. Rahimi-Movaghar, S. U. R. Rahman, M. Raju, I. Rakovac, S. M. Rana, A. Refaat, G. Remuzzi, A. L. Ribeiro, S. Ricci, P. M. Riccio, L. Richardson, J. H. Richardus, B. Roberts, D. A. Roberts, M. Robinson, A. Roca, A. Rodriguez, D. Rojas-Rueda, L. Ronfani, R. Room, G. A. Roth, D. Rothenbacher, D. H. Rothstein, J. T. Rowley, N. Roy, G. M. Ruhago, L. Rushton, S. Sambandam, K. Soreide, M. Y. Saeedi, S. Saha, R. Sahathevan, M. A. Sahraian, B. W. Sahle, J. A. Salomon, D. Salvo, G. M. J. Samonte, U. Sampson, J. R. Sanabria, L. Sandar, I. S. Santos, M. Satpathy, M. Sawhney, M. Saylan, P. Scarborough, B. Schottker, J. C. Schmidt, I. J. C. Schneider, A. E. Schumacher, D. C. Schwebel, J. G. Scott, S. G. Sepanlou, E. E. Servan-Mori, K. Shackelford, A. Shaheen, S. Shahraz, M. Shakh-Nazarova, S. Shangguan, J. She, S. Sheikhbahaei, D. S. Shepard, K. Shibuya, Y. Shinohara, K. Shishani, I. Shiue, R. Shivakoti, M. G. Shrime, I. D. Sigfusdottir, D. H. Silberberg, A. P. Silva, E. P. Simard, S. Sindi, J. A. Singh, L. Singh, E. Sioson, V. Skirbekk, K. Sliwa, S. So, M. Soljak, S. Soneji, S. S. Soshnikov, L. A. Sposato, C. T. Sreeramareddy, J. R. D. Stanaway, V. K. Stathopoulou, K. Steenland, C. Stein, C. Steiner, A. Stevens, H. Stoeckl, K. Straif, K. Stroumpoulis, L. Sturua, B. F. Sunguya, S. Swaminathan, M. Swaroop, B. L. Sykes, K. M. Tabb, K. Takahashi, R. T. Talongwa, F. Tan, D. Tanne, M. Tanner, M. Tavakkoli, B. T. Ao, C. M. Teixeira, T. Templin, E. Y. Tenkorang, A. S. Terkawi, B. A. Thomas, A. L. Thorne-Lyman, A. G. Thrift, G. D. Thurston, T. Tillmann, D. L. Tirschwell, I. M. Tleyjeh, M. Tonelli, F. Topouzis, J. A. Towbin, H. Toyoshima, J. Traebert, B. X. Tran, T. Truelsen, U. Trujillo, M. Trillini, Z. T. Dimbuene, M. Tsilimbaris, E. M. Tuzcu, C. Ubeda, U. S. Uchendu, K. N. Ukwaja, E. A. Undurraga, A. J. Vallely, S. van de Vijver, C. H. van Gool, Y. Y. Varakin, T. J. Vasankari, A. M. N. Vasconcelos, M. S. Vavilala, N. Venketasubramanian, L. Vijayakumar, S. Villalpando, F. S. Violante, V. V. Vlassov, G. R. Wagner, S. G. Waller, J. L.

Wang, L. Wang, X. R. Wang, Y. P. Wang, T. S. Warouw, S. Weichenthal, E. Weiderpass, R. G. Weintraub, W. Wenzhi, A. Werdecker, K. R. R. Wessells, R. Westerman, H. A. Whiteford, J. D. Wilkinson, T. N. Williams, S. M. Woldeyohannes, C. D. A. Wolfe, T. M. Wolock, A. D. Woolf, J. Q. Wong, J. L. Wright, S. Wulf, B. Wurtz, G. L. Xu, Y. C. Yang, Y. Yano, H. Yatsuya, P. Yip, N. Yonemoto, S. J. Yoon, M. Younis, C. H. Yu, K. Y. Jin, M. E. S. Zaki, M. F. Zamakhshary, H. Zeeb, Y. Zhang, Y. Zhao, Y. F. Zheng, J. Zhu, S. Zhu, D. Zonies, X. N. Zou, J. R. Zunt, T. Vos, A. D. Lopez, C. J. L. Murray and G. M. C. D. Colla, *Lancet*, 2015, **385**, 117-171.

3.   World Health Organization, Chronic rheumatic conditions, http://www.who.int/chp/topics/rheumatic/en/).

4.   J. D. Lambeth, K. H. Krause and R. A. Clark, *Seminars in Immunopathology*, 2008, **30**, 339-363.

5.   M. Mittal, M. R. Siddiqui, K. Tran, S. P. Reddy and A. B. Malik, *Antioxid Redox Sign*, 2014, **20**, 1126-1167.

6.   C. A. Hitchon and H. S. El-Gabalawy, *Arthritis Res Ther*, 2004, **6**, 265-278.

7.   X. F. Chen, M. J. Song, B. Zhang and Y. Zhang, *Oxid Med Cell Longev*, 2016, DOI: Artn 1580967

10.1155/2016/1580967.

8.   S. Kossmann, M. Knorr, J. Stratmann, M. Hausding, S. Schuhmacher, S. H. Karbach, M. Schwenk, N. Vogev, E. Schulz, M. Oelze, S. Grabbe, H. Jonuleit, C. Becker, A. Daiber, A. Waisman, T. Munzel and P. Wenzel, *Vasc Pharmacol*, 2012, **56**, 317-317.

9.   X. Y. Li, P. Fang, J. T. Mai, E. T. Choi, H. Wang and X. F. Yang, *J Hematol Oncol*, 2013, **6**.

10.   J. D. Lambeth, *Nat Rev Immunol*, 2004, **4**, 181-189.

11.   N. H. Kim, S. Choi, E. J. Han, B. K. Hong, S. Y. Choi, H. M. Kwon, S. Y. Hwang, C. S. Cho and W. U. Kim, *Eur J Immunol*, 2014, **44**, 2721-2736.

12.   Y. A. Komarova, K. Kruse, D. Mehta and A. B. Malik, *Circulation Research*, 2017, **120**, 179-206.

13.   D. Mehta and A. B. Malik, *Physiol Rev*, 2006, **86**, 279-367.

14.   J. L. Aldons, *Nature*, 2000, **407**, 233.

15.   R. Ross, *Am Heart J*, 1999, **138**, S419-420.

16.   T. S. Hiran, P. J. Moulton and J. T. Hancock, *Free Radical Bio Med*, 1997, **23**, 736-743.

17.   P. J. Moulton, T. S. Hiran, M. B. Goldring and J. T. Hancock, *Brit J Rheumatol*, 1997, **36**, 522-529.

18.   M. A. Jakupec, P. Unfried and B. K. Keppler, *Rev Physiol Biochem Pharmacol*, 2005, **153**, 101-111.

19.   C. Korsvik, S. Patil, S. Seal and W. T. Self, *Chem Commun (Camb)*, 2007, DOI: 10.1039/b615134e, 1056-1058.

20.   E. G. Heckert, S. Seal and W. T. Self, *Environ Sci Technol*, 2008, **42**, 5014-5019.

21.   S. Das, J. M. Dowding, K. E. Klump, J. F. McGinnis, W. Self and S. Seal, *Nanomedicine (Lond)*, 2013, **8**, 1483-1508.

22.   A. Karakoti, S. Singh, J. M. Dowding, S. Seal and W. T. Self, *Chemical Society Reviews*, 2010, **39**, 4422-4432.

23.   M. Mahmoudi, S. Sant, B. Wang, S. Laurent and T. Sen, *Adv Drug Deliver Rev*, 2011, **63**, 24-46.

24.   Wahajuddin and S. Arora, *International Journal of Nanomedicine*, 2012, **7**, 3445-3471.

25.   F. M. McQueen, *Rheumatology*, 2000, **39**, 700-706.

26.   M. Back and G. K. Hansson, *Nat Rev Cardiol*, 2015, **12**, 199-211.

27.   F. Chen, E. B. Ehlerding and W. Cai, *J Nucl Med*, 2014, **55**, 1919-1922.

28.   D. Wang, B. B. Lin and H. Ai, *Pharm Res-Dordr*, 2014, **31**, 1390-1406.

29.   P. Couvreur, *Adv Drug Deliver Rev*, 2013, **65**, 21-23.

30.   S. Ganta, H. Devalapally, A. Shahiwala and M. Amiji, *J Control Release*, 2008, **126**, 187-204.

31.   J. Park, K. J. An, Y. S. Hwang, J. G. Park, H. J. Noh, J. Y. Kim, J. H. Park, N. M. Hwang and T. Hyeon, *Nat Mater*, 2004, **3**, 891-895.

32.   S. Sun and H. Zeng, *J Am Chem Soc*, 2002, **124**, 8204-8205.

33.   T. Zhou, B. Y. Wu and D. Xing, *J Mater Chem*, 2012, **22**, 470-477.

34.   L. L. Pang, J. S. Li, J. H. Jiang, Y. Le, G. L. Shen and R. Q. Yu, *Sensor Actuat B-Chem*, 2007, **127**, 311-316.

35.   X. Wang, T. Yang and K. Jiao, *Biosens Bioelectron*, 2009, **25**, 668-673.

36.   C. M. Yeung, K. M. Yu, Q. J. Fu, D. Thompsett, M. I. Petch and S. C. Tsang, *J Am Chem Soc*, 2005, **127**, 18010-18011.

37.   F. F. Zhu, G. Z. Chen, S. X. Sun and X. Sun, *J Mater Chem A*, 2013, **1**, 288-294.

38.   T. Sugama, L. E. Kukacka and N. Carciello, *J Mater Sci*, 1984, **19**, 4045-4056.

39.   T. Pirmohamed, J. M. Dowding, S. Singh, B. Wasserman, E. Heckert, A. S. Karakoti, J. E. S. King, S. Seal and W. T. Self, *Chemical Communications*, 2010, **46**, 2736-2738.

40.   F. Y. Cheng, C. H. Su, Y. S. Yang, C. S. Yeh, C. Y. Tsai, C. L. Wu, M. T. Wu and D. B. Shieh, *Biomaterials*, 2005, **26**, 729-738.

41.   H. T. Ta, Z. Li, C. E. Hagemeyer, G. Cowin, S. Zhang, J. Palasubramaniam, K. Alt, X. Wang, K. Peter and A. K. Whittaker, *Biomaterials*, 2017, **134**, 31-42.

42.   H. Ta, Z. Li, C. Hagemeyer, G. Cowin, J. Palasubramaniam, K. Peter and A. Whittaker, *Atherosclerosis*, 2017, **263**, E146-E146.

43.   H. T. Ta, Z. Li, Y. Wu, G. Cowin, S. H. Zhang, A. Yago, A. K. Whittaker and Z. P. Xu, *Materials Research Express*, 2017, **4**.

44.   H. Ta, S. Prabhu, E. Leitner, F. Jia, K. Putnam, N. Bassler, K. Peter and C. Hagemeyer, *Atherosclerosis*, 2015, **241**, E26-E26.

45.   H. T. Ta, S. Prabhu, E. Leitner, F. Jia, D. von Elverfeldt, K. E. Jackson, T. Heidt, A. K. N. Nair, H. Pearce, C. von zur Muhlen, X. Wang, K. Peter and C. E. Hagemeyer, *Circulation Research*, 2011, **109**, 365-373.

46.   H. T. Ta, S. Prabhu, E. Leitner, F. Jia, K. Putnam, N. Bassler, K. Peter and C. Hagemeyer, *Circulation Research*, 2010, **107**, e37-e38.

47.   A. Tsourkas, V. R. Shinde-Patil, K. A. Kelly, P. Patel, A. Wolley, J. R. Allport and R. Weissleder, *Bioconjugate Chem*, 2005, **16**, 576-581.

48.   A. Mirshafiey and M. Mohsenzadegan, *Iran J Allergy Asthm*, 2008, **7**, 195-202.

49.   S. M. Hirst, A. S. Karakoti, R. D. Tyler, N. Sriranganathan, S. Seal and C. M. Reilly, *Small*, 2009, **5**, 2848-2856.

50.   D. Schubert, R. Dargusch, J. Raitano and S. W. Chan, *Biochem Bioph Res Co*, 2006, **342**, 86-91.

51.   A. Clark, A. P. Zhu, K. Sun and H. R. Petty, *J Nanopart Res*, 2011, **13**, 5547-5555.

52.   T. Shirai, M. Hilhorst, D. G. Harrison, J. J. Goronzy and C. M. Weyand, *Autoimmunity*, 2015, **48**, 139-151.

53.   P. R. Taylor, L. Martinez-Pomares, M. Stacey, H. H. Lin, G. D. Brown and S. Gordon, *Annu Rev Immunol*, 2005, **23**, 901-944.

54.   R. W. Kinne, R. Brauer, B. Stuhlmuller, E. Palombo-Kinne and G. R. Burmester, *Arthritis Res*, 2000, **2**, 189-202.

55.   World Healyh Organization, Cardiovascular diseases (CVDs), http://www.who.int/mediacentre/factsheets/fs317/en/).

56.   R. P. Patel, D. Moellering, J. Murphy-Ullrich, H. Jo, J. S. Beckman and V. M. Darley-Usmar, *Free Radic Biol Med*, 2000, **28**, 1780-1794.

57.   H. Sakurai, H. Kohsaka, M. F. Liu, H. Higashiyama, Y. Hirata, K. Kanno, I. Saito and N. Miyasaka, *J Clin Invest*, 1995, **96**, 2357-2363.

58.   A. Karakoti, S. Singh, J. M. Dowding, S. Seal and W. T. Self, *Chem Soc Rev*, 2010, **39**, 4422-4432.

59.   J. M. Dowding, S. Das, A. Kumar, T. Dosani, R. McCormack, A. Gupta, T. X. T. Sayle, D. C. Sayle, L. von Kalm, S. Seal and W. T. Self, *Acs Nano*, 2013, **7**, 4855-4868.

60.   Wilhelm, C. Billotey, J. Roger, J.N. Pons, J.C. Bacri, F. Gazeau, *Biomaterials*, 2003 24 1001-1011.

61.   L.K. Limbach, Y.C. Li, R.N. Grass, T.J. Brunner, M.A. Hintermann, M. Muller, D. Gunther, W.J. Stark, *Environmental Science & Technology* 2005 **39** 9370-9376.

62.   S. Patil, A. Sandberg, E. Heckert, W. Self, S. Seal, *Biomaterials* 2007 **28** 4600-4607.

63.   Y. Tabata, Y. Ikada, *Biomaterials* 1988 **9** 356-362.

64.   C.J. Chen, H.Y. Lai, C.C. Lin, J.S. Wang, R.K. Chiang, *Nanoscale Res Lett* 2009 **4** 1343-50.

65.   V.V. Khutoryanskiy, A.V. Dubolazov, Z.S. Nurkeeva, G.A. Mun, *Langmuir* 2004 **20** 3785-3790.

66.   J.T. Dahle, K. Livi, Y. Arai, *Chemosphere* 2015 **119** 1365-1371.

67.   S. Bae, M. Park, C. Kang, S. Dilmen, T.H. Kang, D.G. Kang, Q. Ke, S.U. Lee, D. Lee, P.M. Kang, *J Am Heart Assoc* 2016 **5**.

68.   X. Liu, W. Wei, Q. Yuan, X. Zhang, N. Li, Y. Du, G. Ma, C. Yan, D. Ma*, Chemical Communications* 2012 **48** 3155-3157..

69.   S.M. Hirst, A.S. Karakoti, R.D. Tyler, N. Sriranganathan, S. Seal, C.M. Reilly, *Small* 2009 **5** 2848-56.

Novel iron oxide-cerium oxide core-shell nanoparticle as a potential theranostic material for ROS related inflammatory diseases

TOC Graphic
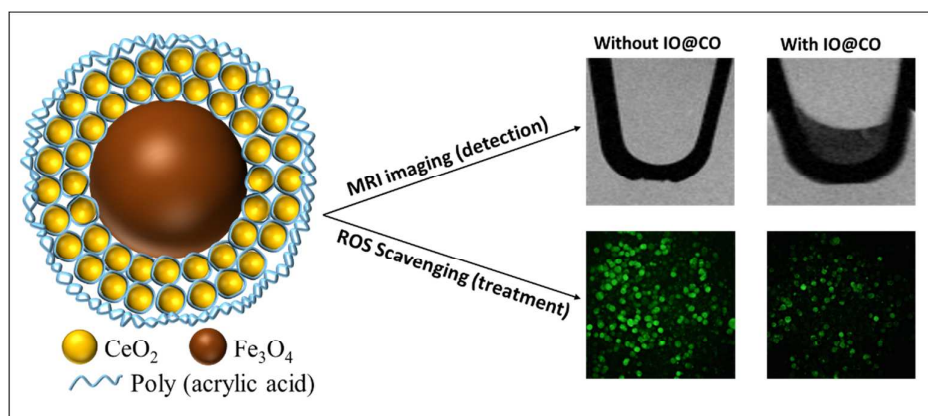
Novel iron oxide-cerium oxide core-shell theranostic nanoparticle for MRI imaging and ROS scavenging effects.